Guidance document on the in-beam X-ray spectrometry of reference radiation fields in laboratories using germanium and cadmium telluride detectors

Funded by the European Union. Views and opinions expressed are however those of the author(s) only and do not necessarily reflect those of the European Union or EURAMET. Neither the European Union nor the granting authority can be held responsible for them.

The project has received funding from the European Partnership on Metrology, co-financed from the European Union's Horizon Europe Research and Innovation Programme and by the Participating States.

Contents

1. Preface

This guide was compiled by Gerhard Hilgers for germanium (Ge) spectrometers and the spectrometry issues in general and subsequently updated by Jaroslav Šolc with information specific to cadmium telluride (CdTe) spectrometers.

2. Introduction

The spectral distribution of the photons of radiation qualities produced in X-ray facilities builds the basis for the determination of various characteristics of the respective radiation quality like mean photon energy, kerma factor or conversion coefficients for radiation protection quantities. Due to slight variations in setup, filter materials and thickness, state of the X-ray tube (age, anode roughness, …) and technique to generate the operation voltage, the facilities to produce these fields are not perfectly identical but rather are “individuals”. Therefore, also the X-ray spectra produced by the different facilities are not perfectly identical. In consequence, spectrometric characterisation of the X-ray fields is required for a solid determination of the corresponding dosimetric quantities. The characterisation is carried out by spectrometry using appropriate radiation detectors.

The golden standard of X-ray and γ-ray spectrometry is a detector with the sensing element made of high-purity germanium (HPGe; Ge-detectors). The crystals can be manufactured large, which, in combination with the high proton number and density, allows for high relative detection efficiency even for high-energy photons (> 1 MeV). Stability at low temperature and excellent energy resolution make them ideal spectrometers for laboratories. On the other hand, they are bulky and, typically, difficult to transport. Another detector suitable for X-ray spectrometry makes use of a different semiconductor material – cadmium telluride (CdTe). This material allows the manufacture of small sensors only, which, at the end, enables the production of small, easy-to-transport detectors. The small size of the sensor is not a disadvantage but rather a benefit for measurements at high flux beams. Also, the sensor is usually cooled down for improved energy resolution, but not to such a low temperature as the HPGe, therefore the cooler is much smaller, supporting the compactness of the device. The detector is ready for measurements once powered on. Such detectors have slightly worse spectrometric properties than the HPGe ones but provide a possibility to perform in-beam X-ray spectrometry outside the laboratory, e.g., at clinics or defectoscopy workplaces. Setting up the measurement can be achieved in less than one hour. Disassembly of the setup requires about 10 min.

This guide describes the in-beam spectrometry of X-ray radiation qualities in general but is more focused on Ge-detectors. Information specific to CdTe detectors only, namely to the X-123CdTe spectrometer from Amptek, Inc., USA, is given whenever appropriate.

3. Factors affecting the photon spectrum quality

3.1 General

The quality of the recorded pulse height spectra is influenced by several factors:

- Alignment of detector, collimator and X-ray source,
- Choice of the count rate in the detector,

- Energy calibration of the detector,
- Detector shielding against scattered radiation,
- Photon background due to cosmic and terrestrial radiation incident on the detector,
- Charge carrier transport in CdTe detectors,
- Choice of pulse shaping times in the data acquisition, depending on the count rate in the detector,
- Statistics of counts in energy channels.

Therefore, it is mandatory to ensure a proper setup and a proper choice of parameters in the data acquisition during a spectrometry campaign.

For the present investigation, pulse height spectra were recorded with a Ge-detector followed by a digital pulse processor, or with a CdTe spectrometer with integrated digital pulse processor. The recorded pulse height spectra were unfolded (see section 4.2) to obtain the corresponding fluence spectra of the incident photon radiation. Based on these unfolded spectra, selected dosimetric quantities and conversion coefficients were determined.

All unfolded spectra of the Ge-detector shown in this document are normalised to an integral of unity.

3.2 Alignment of detector, collimator and X-ray source

Generally, the intensities of radiation fields produced by X-ray facilities are by far too high to allow for spectrometry using single photon counting detectors without additional measures to reduce the intensity of the radiation incident on the detector. Typically, the detector is enclosed by a radiation shield surrounding the detector at its front and sides, protecting the detector from scattered and direct radiation (see also section 3.5), and the photons enter the detector through a small aperture in the front of the radiation shield. Technically, the apertures are made as insets (or disks) into a larger opening in the front of the radiation shield to allow for a quick variation of the aperture diameter by exchanging the insets. The diameter of these aperture insets can range from tens of micrometres to millimetres. For X-ray beams above ~150 keV, their thickness is in the order of several centimetres (for CdTe, several mm, plus additional shielding) to preserve proper shielding, therefore, as side effect, the apertures also act as collimators. Consequently, it is mandatory to ensure that both the central axis of the collimating aperture and the propagation direction of the photons emitted from the X-ray source, do coincide. Otherwise, photons entering the collimating aperture hit its inner walls and may produce artefacts, which superpose the primary photon spectrum and with it deteriorates the measured pulse height spectrum.

The first step in the alignment procedure is to position the collimating aperture on the central axis of the radiation field using the laser, which usually is used to align the devices, which are to be irradiated, on the central axis of the radiation field, as shown in Fig. 1. The aperture entrance is close to the centre of the red spot corresponding to the alignment laser. Fig. 2 shows the collimation system for a CdTe spectrometer.

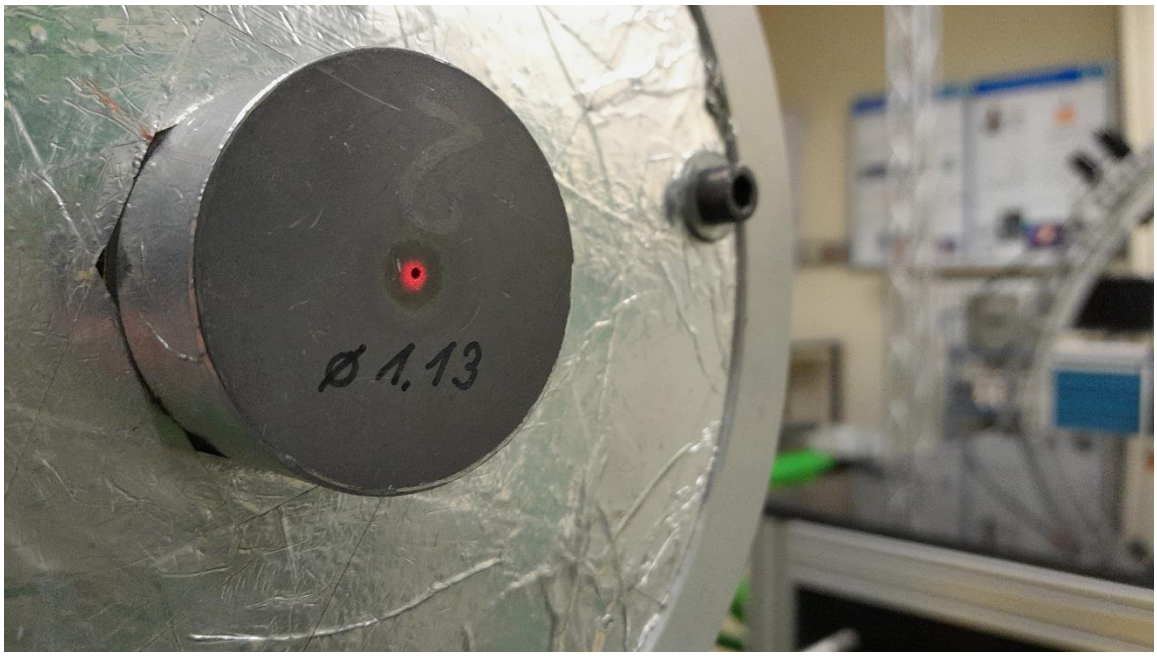

Fig. 1: Setup for Ge-spectrometry. Positioning of the collimating aperture on the central axis of the radiation field. The aperture/collimator entrance is close to the centre of the red spot marking the alignment laser.

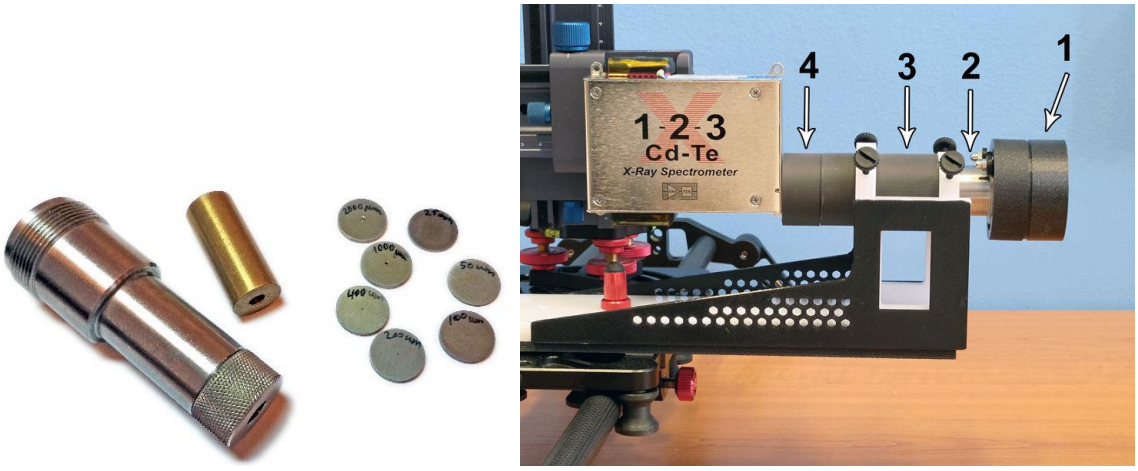

Fig. 2: Setup for CdTe spectrometry. Left – steel collimator with a set of tungsten collimation disks with apertures of various diameters. Disk diameter is 1.6 cm. Right: CdTe detector inside a shielded collimator. Metal box height is 7 cm. 1 - extension front lead collimator (for energies > 150 keV); 2 - front tungsten collimator; 3 - lateral shielding; 4 - rear shielding. Diameter of the shielding (parts 3 and 4) is 38 mm.

The second step is to align the collimating aperture such that its central axis coincides with the propagation direction of the photons emitted from the X-ray source. This step can be carried out by different methods, e.g.

- Using the diffraction pattern produced by the light of the same alignment laser. This method is demonstrated in the following text and Fig. 3 on the alignment of a Ge-detector.

- Using a projection of two pinholes on a pixelized detector. This method is demonstrated in detail in [1] for a CdTe detector and summarized also here in the further text. The estimated accuracy of the alignment is 0.2°.

Fig. 3 shows diffraction patterns of the collimating aperture for different angles of a horizontal misalignment of its central axis with respect to the propagation direction of the photons emitted from the X-ray source on a sheet of paper fixed at the wall behind. With increasing angle of misalignment, the diffraction pattern deviates increasingly from a circular pattern, which is found for vanishing misalignment (see Fig. 3a), towards an elliptical diffraction pattern with horizontal semi-major axis. A vertical misalignment will show an elliptical diffraction pattern with vertical semi-major axis.

As extra verification, it is expected that the maximum counting rate of the detector is obtained when the central axis of the collimator coincides with the propagation direction of the photons.

Fig. 4 demonstrates the alignment for a CdTe spectrometer using a projection of two pinholes on a pixelized detector. With the increasing angle of misalignment, the distance between the projection of two pinholes increases. More details are given in [1].

To investigate the effects of misalignment, pulse height spectra of selected radiation qualities were recorded with a Ge-detector for angles of misalignment as mentioned in Fig. 3, i.e. 0°, 0.25°, 0.5° and 0.75°. In addition, pulse height spectra were recorded for an angle of 1.1°.

For this angle the relative shift between entrance and exit opening of the collimating aperture corresponds to the diameter of these openings. Consequently, the primary photon radiation cannot pass the collimating aperture.

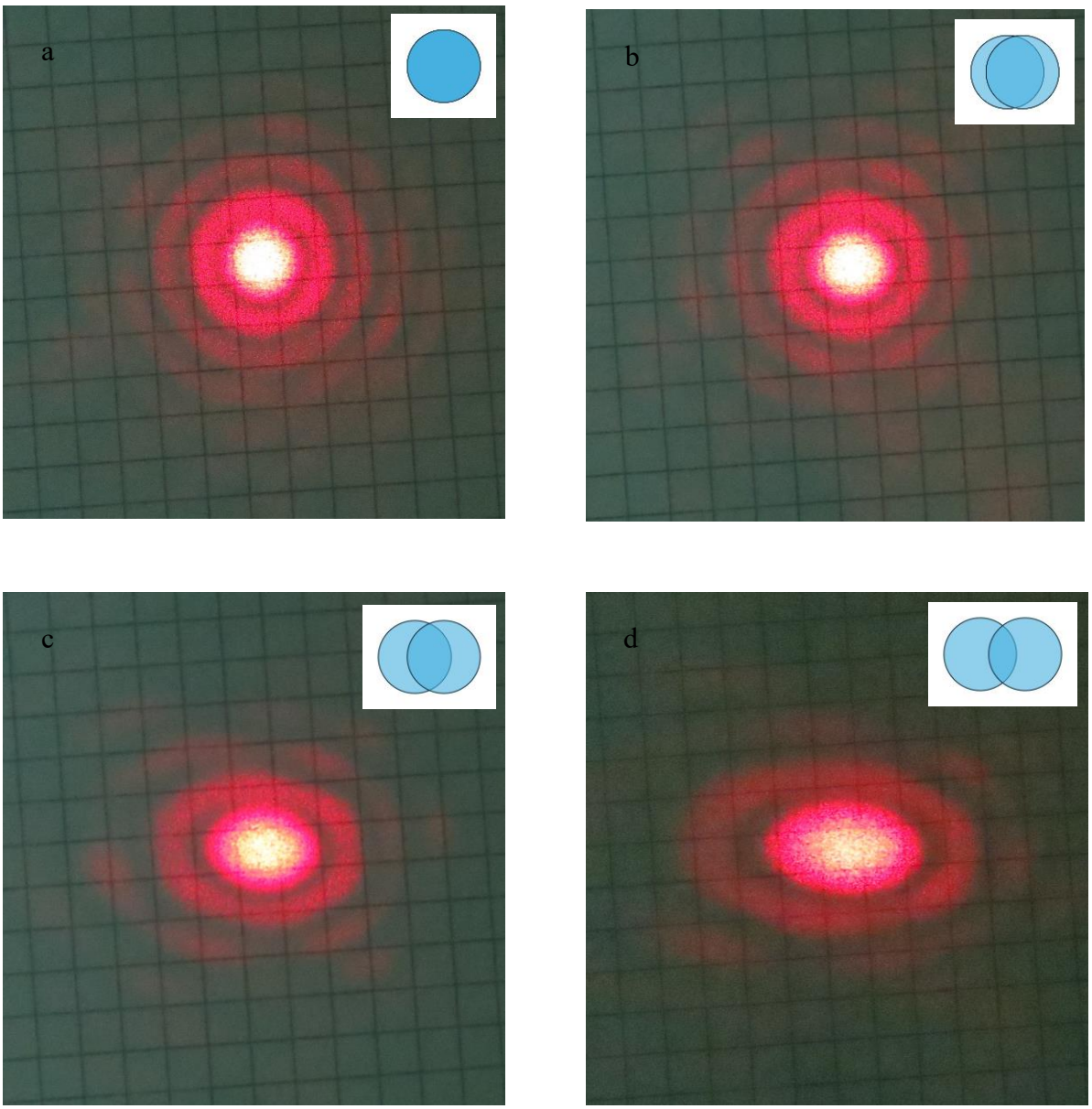

Fig. 3: Diffraction patterns of the collimating aperture for different angles of misalignment (a: 0°, b: 0.25°, c: 0.5°, d: 0.75°) of its central axis with respect to the propagation direction of the photons emitted from the X-ray source. Diameter and length of the collimating aperture are 1.13 mm and 60 mm, respectively. The insets represent the relative shift between entrance and exit opening of the collimating aperture with respect to the propagation direction of the photons emitted from the X-ray source. The size of the squares on the paper sheet is 5 mm × 5 mm, the distance between collimating aperture and paper sheet is in the order of 8 m.

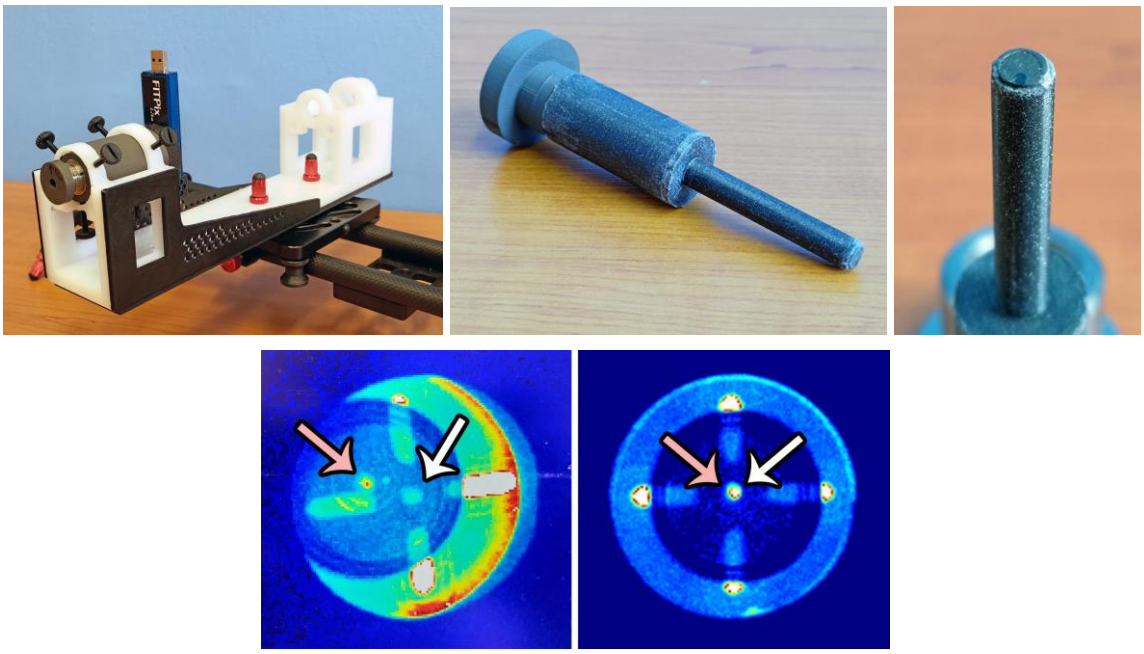

Fig. 4: Setup for CdTe spectrometry. Top: Inset for accurate alignment of the steel collimator axis towards the X-ray tube focus point; it is inserted into the steel collimator, in front of a pixelized detector. Bottom: Projection of the two apertures on the alignment inset; left – the steel collimator is not aligned, pinholes projected to different places; right – the collimator is aligned, pinholes projected to the same place.

The effect of the misalignment of the collimating aperture's central axis and the propagation direction of the photons emitted from the X-ray source on the unfolded photon spectra and the derived quantities for the radiation qualities N-60 and N-200 is shown in Fig. 5 and Fig. 9, respectively.

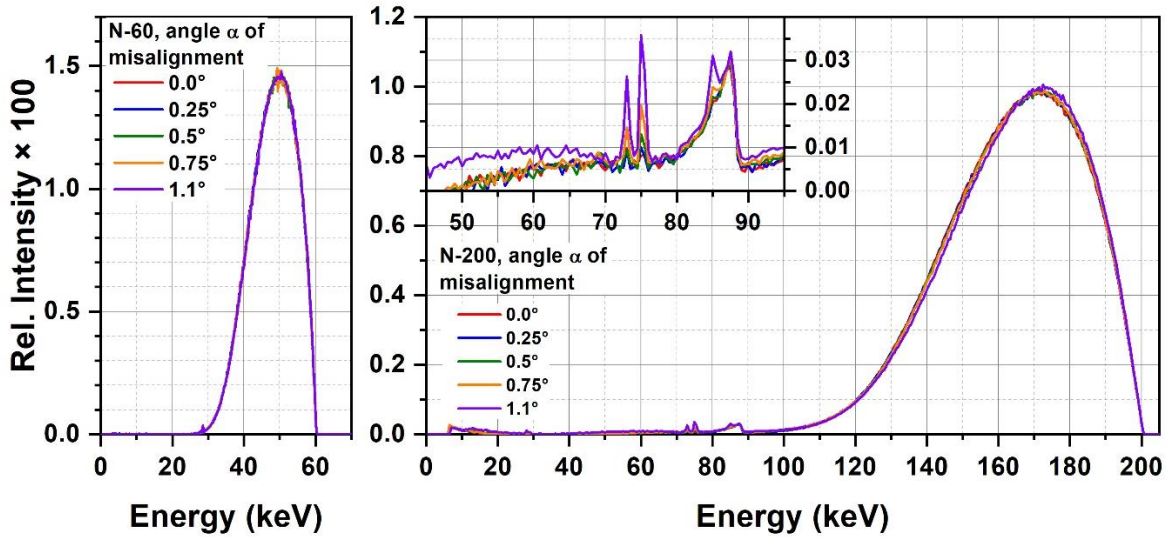

Fig. 5: Unfolded photon fluence spectra of radiation qualities N-60 (left) and N-200 (right) for different angles α of misalignment of the collimating aperture.

For N-60 all unfolded spectra coincide, i.e. no effect of the misalignment on the unfolded spectra can be observed. For the high energy range of N-200, a slight shift of the intensity

distribution towards higher energies can be observed for an angle of misalignment of 1.1° due to radiation hardening, which is caused by the stronger attenuation of photons of lower energies in the collimating aperture's walls. In the low energy range of N-200 (inset in the right plot of Fig. 5) an increase of the intensity of the Pb fluorescence (73 keV ($K_{\alpha 2}$), 75 keV ($K_{\alpha 1}$), 85 keV ($K_{\beta 1}$)) is observed with increasing angle of misalignment. Moreover, for an angle of misalignment of 1.1° the intensity of photons of energies below 70 keV increases.

Both effects are due to primary photons hitting the collimating aperture's walls and producing low energy scattered photons and fluorescence photons.

A similar study was performed in [1] for the geometry used with CdTe detectors. Due to the very small diameter of apertures (≥ 25 μm) and tungsten hardness, the process of making the holes into tungsten is different. It is often done by laser drilling or sparking, which may result in inclined holes with respect to the normal to the surface of the disk. Therefore, a combination of two effects may occur that leads to the same effect of deformed measured spectra described above (Fig. 6):

- Misalignment of the collimator axis,
- Tilt of the aperture axis.

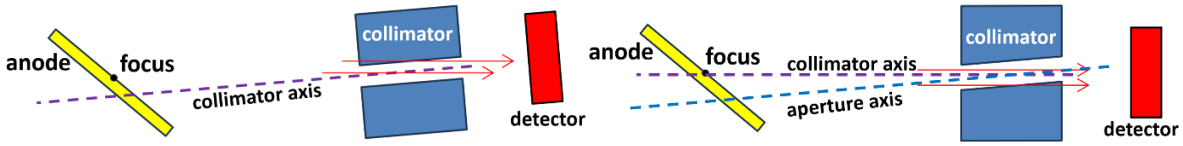

Fig. 6: Schematics of processes leading to deformation of measured spectra: misalignment of collimator axis (left) and the tilt of the aperture axis (right).

The alignment of the collimator axis can be achieved using, e.g., the projection of two pinholes described in the previous text. The tilt of the aperture axis can be either solved by characterisation of the collimation disk, or by using a disk where this effect is negligible. The latter typically means to use a disk with a large aperture, i.e., ≥ 200 μm diameter (for a disk thickness of 2 mm). Characterisation of the collimation disk can be performed by modifying the aperture geometry in the Monte Carlo model until the agreement of measured and simulated pulse height spectra is achieved. As an example, Fig. 7 presents the pulse height spectra measured with small and large apertures and the simulated spectrum for a tilt of the aperture such that it achieves the same shape of the pulse height spectrum. The optimised MC model was subsequently used for calculation of the response matrix for unfolding to compensate for this effect. In order for the corrections to be efficient, both effects have to be solved simultaneously – the alignment has to be accurate, and the apertures have to be characterised. Details are presented in [1].

Fig. 8 shows the unfolded spectra determined with the former alignment method and without considering the tilt, and after corrections to both effects were optimised.

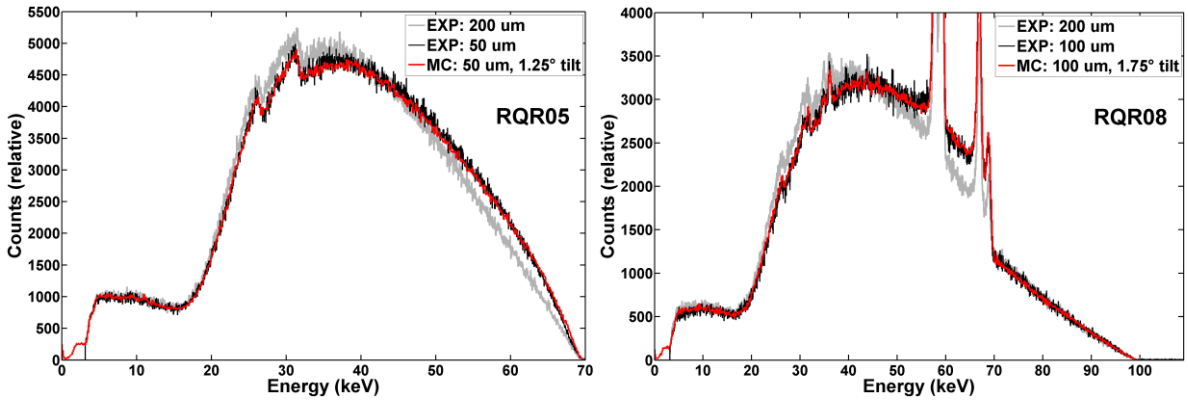

Fig. 7: Comparison of measured pulse height spectra of RQR05 and RQR08 beam qualities (black) with the simulated pulse height spectra (red) for a tilt angle of 1.25° and 1.75° between the aperture axis of the collimation disk with 50 µm (left) and 100 µm (right) diameter aperture, respectively, and the steel collimator axis. Pulse height spectra acquired with a larger aperture diameter disk (grey; no influence on the shape of pulse height spectra) are shown for comparison. The spectra were normalized to the same area.

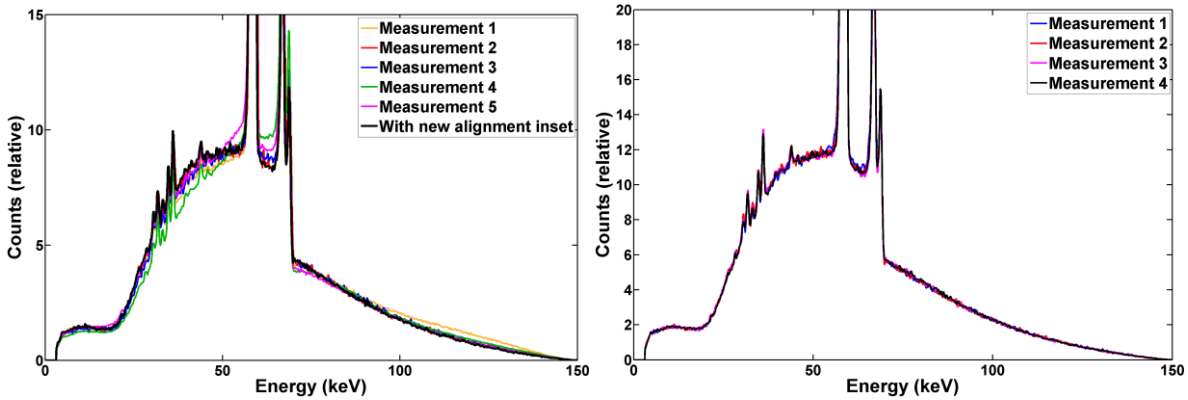

Fig. 8: Reproducibility of RQR10 pulse height spectrum measured with 100 µm aperture diameter collimation disk after positioning the steel collimator with the laser pointer (left; measurements in years 2020-2024) and with the new alignment tool (right; different measurement sessions). Spectra were normalized to their area and were smoothed for better readability.

The dosimetric quantities and conversion coefficients (Fig. 9) derived from unfolded photon fluence spectra of both radiation qualities N-60 and N-200 measured with the Ge-detector show an increasing deviation from the value obtained for an angle of misalignment of 0° with increasing angle of misalignment of ±0.5% for N-60 and ±0.65% for N-200, respectively, when calculated for the total spectral range. Restricting the spectral range to photon energies of significant intensity (i.e. the energy range between the low energy cut-off caused by the filtering and the energy corresponding to the X-ray tube's operation voltage, see also 3.3) substantially reduces these deviations, especially for angles of misalignment below 0.75°.

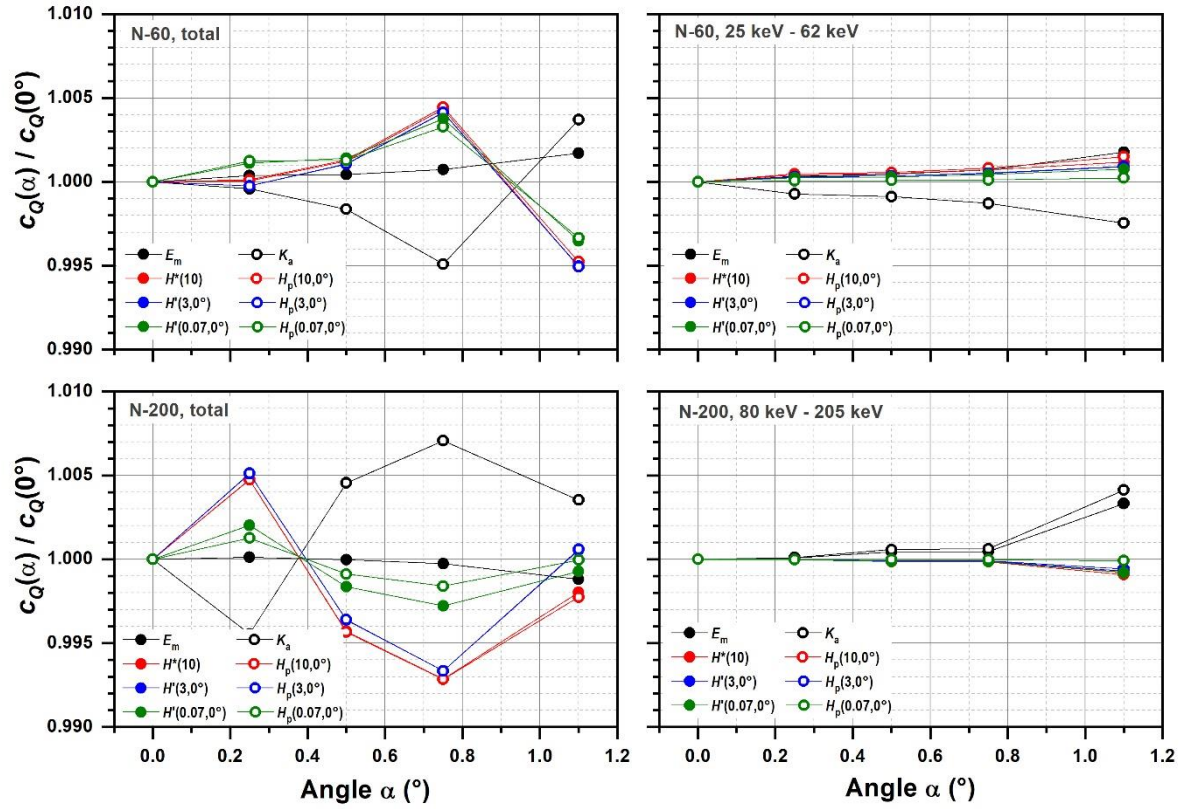

Fig. 9: Selected dosimetric quantities and conversion coefficients derived from unfolded fluence spectra of radiation qualities N-60 (top) and N-200 (bottom) for different angles α of misalignment normalised to the value obtained for an angle of misalignment of 0°. The plots show quantities and coefficients calculated for the total spectral range (left) and for the spectral range restricted to photon energies of significant intensity (right) as indicated.

The effect of the misalignment of the collimating aperture's central axis on the unfolded photon spectra and the derived quantities for the radiation qualities H-150 and H-300 are shown in Fig. 10 and Fig. 11, respectively.

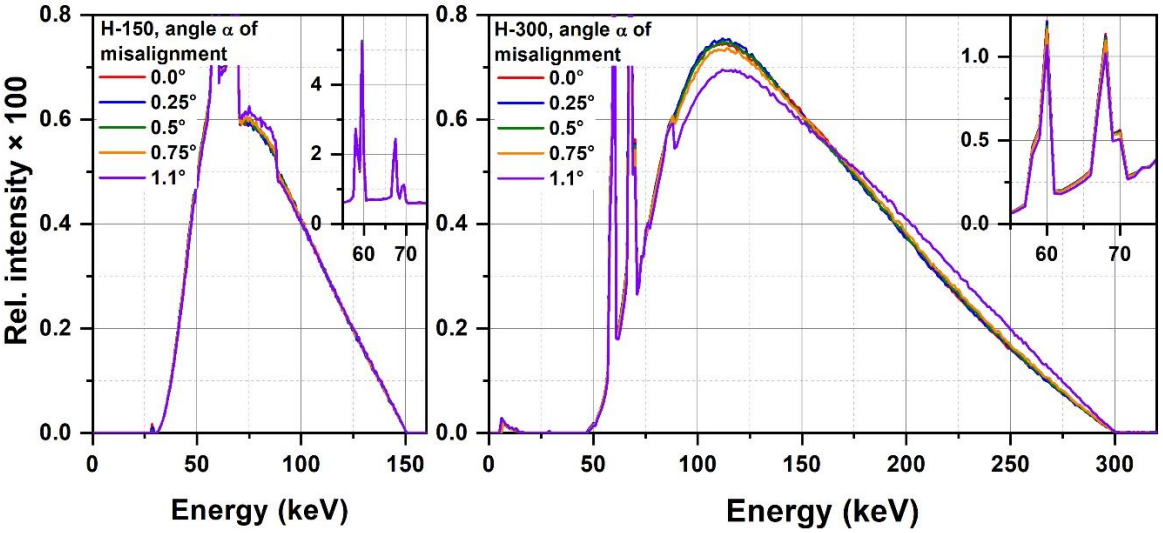

Fig. 10: Unfolded photon fluence spectra of radiation qualities H-150 (left) and H-300 (right) for different angles α of misalignment of the collimating aperture.

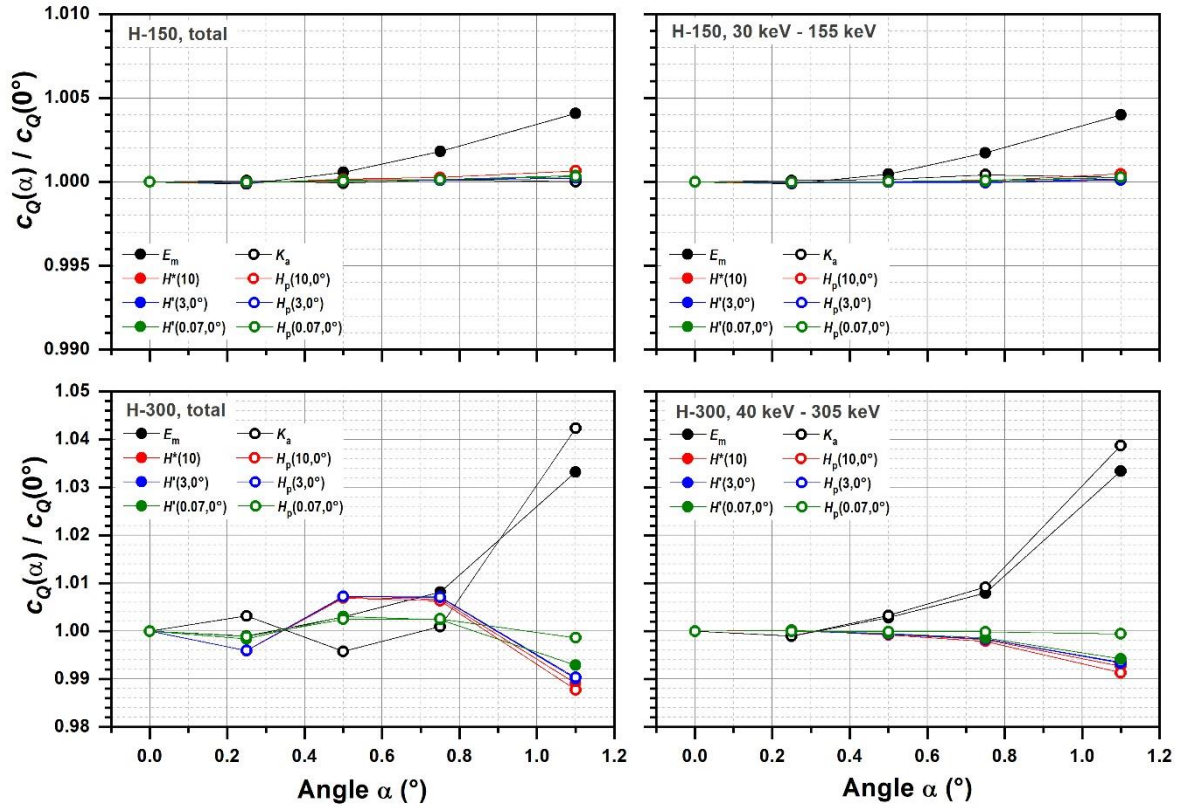

Fig. 11: Selected dosimetric quantities and conversion coefficients derived from unfolded spectra of radiation qualities H-150 (top) and H-300 (bottom) for different angles α of misalignment normalised to the value obtained for an angle of misalignment of 0°. The plots show quantities and coefficients calculated for the total spectral range (left) and for the spectral range restricted to photon energies of significant intensity (right) as indicated. Note the different ranges of the ordinates for H-150 and H-300.

For H-150, changes in association with the K-absorption edge of Pb (88 keV) in the unfolded spectrum are observable for the different angles of misalignment: the larger the angle of misalignment, the larger is the step in the photon intensity at the absorption edge. However, the angle of misalignment has no effect on the intensity of the W fluorescence radiation (inset in the left plot of Fig. 10) emitted from the X-ray tube's anode. For the unfolded spectrum of H-300, the effect of the misalignment is much more pronounced. As for H-150, the step in the photon energy increases with increasing angle of misalignment. Moreover, for an angle of misalignment of 1.1° a significant hardening is observed in the unfolded spectrum, and the intensity of the W fluorescence radiation (inset in the right plot of Fig. 10) decreases with increasing angle of misalignment. The different energy resolution of the W fluorescence radiation in the two insets is due to the different energy resolution of 500 eV (H-150) and 1 keV (H-300) used in the unfolding process (i.e. for the response matrix).

The dosimetric quantities and conversion coefficients (Fig. 11) derived from unfolded spectra show for H-150 a deviation of less than 0.4% from the value obtained for an angle of misalignment of 0° when calculated for the total spectral range. Restricting the spectral range to photon energies of significant intensity substantially reduces these deviations except for the mean photon energy. For H-300 and angles of misalignment up to 0.75°, the corresponding quantities and coefficients differ by less than +0.8% and −0.4% from the value obtained for an angle of misalignment of 0° when calculated for the total spectral range. Restricting the spectral range to photon energies of significant intensity reduces these deviations only for angles of misalignment up to 0.25°. For an angle of misalignment of 1.1° for both, the total range and the

restricted range, large deviations of +4.2% and −1.2% are observed from the value obtained for an angle of misalignment of 0°.

Investigations with a similar scope were performed for the setup with the CdTe detector, resulting in similar findings. Results are presented in [1] and [2].

The misalignment of the collimating aperture's central axis and the propagation direction of the photons emitted from the X-ray source leads to three different types of artefacts in the unfolded photon fluence spectra:

- Additional low-energy scattered radiation and fluorescence radiation due to primary photons hitting the collimating aperture's walls,
- Appearance of the absorption edge of the collimating aperture's material,
- Hardening of the radiation field,
- Reduction of the effective area of the collimator hole (this affects the absolute fluence and air kerma values with all qualities but does not influence the CCs or HVL).

In most cases the misalignment has only a minor effect on the derived dosimetric quantities and conversion coefficients: the deviation of the corresponding quantities and coefficients from the value obtained for an angle of misalignment of 0° is well below 1% when calculated for the total spectral range. However, restricting the spectral range to photon energies of significant intensity reduces these deviations substantially and is therefore recommended in the processing of the unfolded spectra. Moreover, an angle of misalignment of the collimating aperture's central axis and the propagation direction of the photons emitted from the X-ray source of less than 0.5° is recommended to obtain photon spectra of solid quality.

3.3 Count rate in the detector

Due to the time required for processing the charge pulses created by the X-ray photons in the detector, the rate of the photons incident on the detector generating the detected counts affects the measured pulse height spectra. Fig. 12 shows the effect of the dead time on the unfolded fluence spectra caused by different count rates for selected radiation qualities.

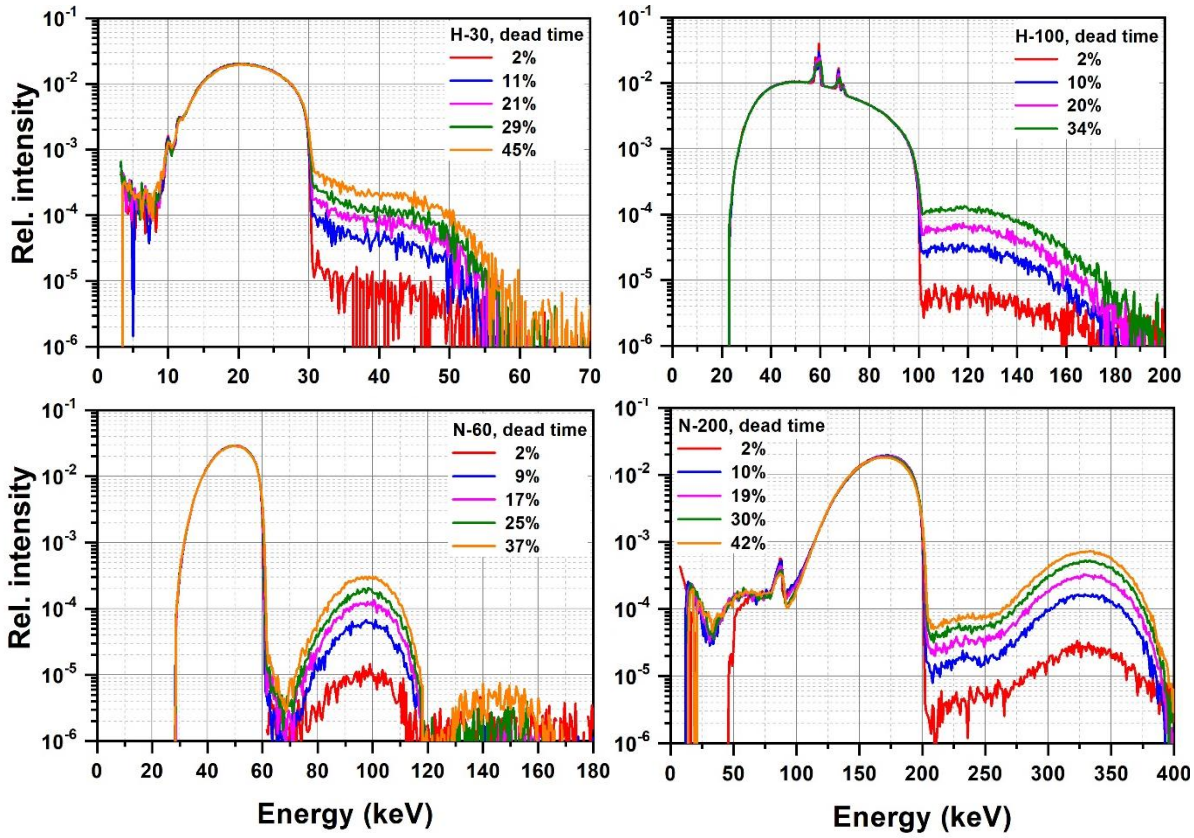

Fig. 12: Unfolded fluence spectra of selected radiation qualities for different dead times (i.e. different count rates) measured with a Ge-detector followed by a digital pulse processor. Top left: H-30, top right: H-100, bottom left: N-60, bottom right: N-200.

The spectra were recorded with a Ge-detector followed by a digital pulse processor. The output pulses of the charge sensitive preamplifier incorporated inside the housing of the Ge-detector are shaped trapezoidally by the digital pulse processor with defined rise (fall) time of the rising (falling) edge and flat-top time of the trapezoid, where rise time and fall time are identical. The resulting dead time depends on the count rate and is shown in Fig. 13 for rise/fall times of 5.6 µs and a flat-top time of 1.2 µs.

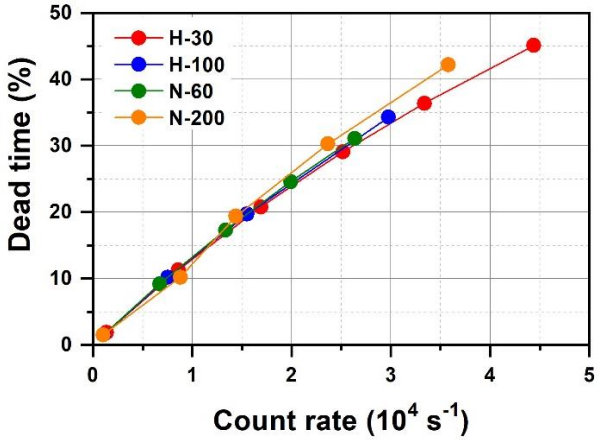

Fig. 13: Dead time of the Ge-detector, indicated by the acquisition software, in dependence on the count rate for selected radiation qualities for trapezoidally shaped pulses with rise/fall times of 5.6 µs and flat-top time of 1.2 µs. The dead time is expected to be energy independent. The small differences observed are probably similar to the associated uncertainties of the dead time.

When the time interval between two photons successively interacting in the detector is sufficiently short, the two photon pulses are not separated by the data processing system but rather processed as one single pulse with the two energies deposited by the two photons summed up. Consequently, in the pulse height spectrum a count is registered at the summation energy. This process is denoted as pile-up and its effect is clearly visible in the energy range above the maximum energy of the photons emitted by the X-ray tube, which is determined by the high voltage applied to the X-ray tube.

The artefacts due to pile-up appear as additional structures in the unfolded fluence spectra (Fig. 12). In the range above the maximum photon energy of the primary radiation field all unfolded spectra show a continuum of photon energies with intensity increasing with dead time, i.e. with count rate. As these continua are due to the summation of the energies of primary photons, they reflect to some extent the intensity distribution of the primary radiation field. This can be seen best in the photon spectra of N-60 and N-200. Here the artefacts due to pile-up are peak shaped with widths similar to the primary radiation fields and with intensity maxima at energies close to twice (and even triple for N-60) the energy at the maximum intensity of the primary radiation.

Besides the production of artefacts, pile-up can deteriorate structures present in the photon spectra. Fig. 14 shows details in the pulse height spectra of H-100 and N-200 for different count rates (i.e. different dead times).

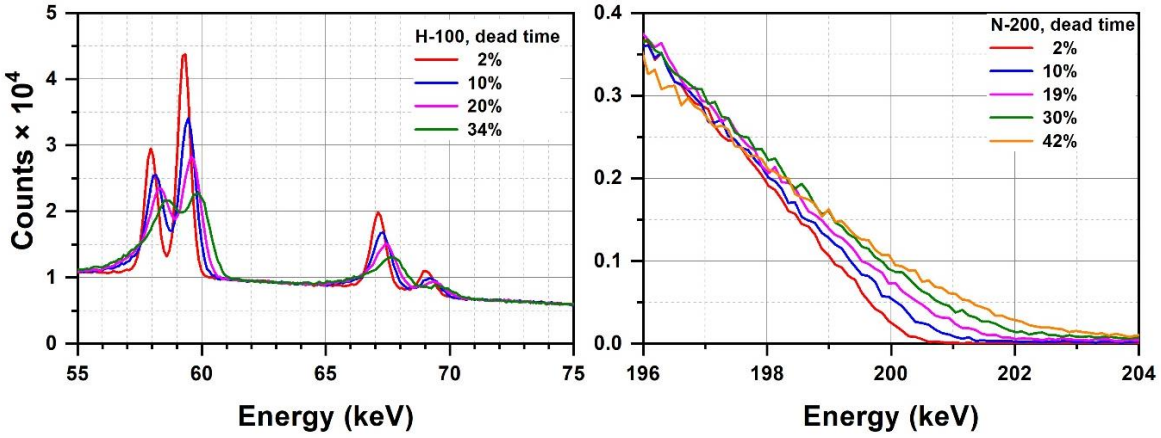

Fig. 14: Details of the pulse height spectra of H-100 (left) and N-200 (right) for different dead times (i.e. different count rates) measured with the Ge-detector.

The number of counts is identical in the pulse height spectra of each radiation quality. The plot for H-100 (left) shows the W fluorescence lines of the X-ray tube's anode. For low count rate, the emission lines are well resolved and significantly more intense than the bremsstrahlung of the radiation field. With increasing count rate, both the intensity of the W fluorescence lines, and the energy resolution of the detection system decrease and the fluorescence lines shift towards higher energies. Moreover, as shown in the plot for N-200 (right), the pulse height spectrum close to the maximum photon energy of the radiation field, which corresponds to the high voltage applied to the X-ray tube, is increasingly blurred and shifted towards higher energy with increasing count rate, making it harder (or even impossible) to determine the maximum photon energy of the radiation field.

The same influence of the count rate on the detector response can be observed with CdTe detectors as well. As an example, Fig. 15 presents the influence of the count rate on the shape of the 122 keV full-energy peak and the dead time dependence on the total count rate for various

radionuclide and X-ray radiation qualities. The count rate also has an influence on energy calibration and on the effect of the incomplete charge collection in the sensor.

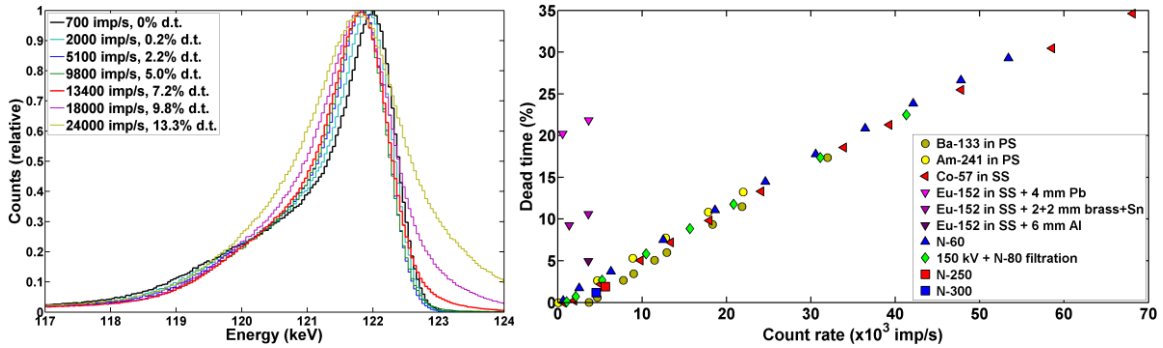

Fig. 15: Left - position and shape of the 122 keV full-energy peak of ^{57}Co (right) acquired at various detector total count rates in pulses per second (imp/s), and the corresponding dead times (d.t.). Right - detector dead time as a function of the detector total count rate for various X-ray qualities and radionuclide sources. PS stands for polystyrene, SS for stainless steel.

That is why the preferable solution is to select a fixed value of the count rate, for which the spectrometry will always be performed, if it is possible. For the detector settings presented in [1], the preferred count rate is 13 000 imp/s, which is a compromise between accuracy of pulse height spectrum acquisition and the acquisition time. If the spectrum does not have characteristic peaks, the count rate can be up to double, because the deterioration of the energy resolution and the pile-ups have negligible influence on the pulse height spectrum shape. If such a count rate is fixed, the corresponding air kerma rate, K_a rate, depends on the X-ray spectrum mean energy and the diameter of the collimation disk aperture as shown in Fig. 16. This can help to estimate whether spectrometry is possible for the given radiation quality and exposure parameters. More details are given in [1] and [2].

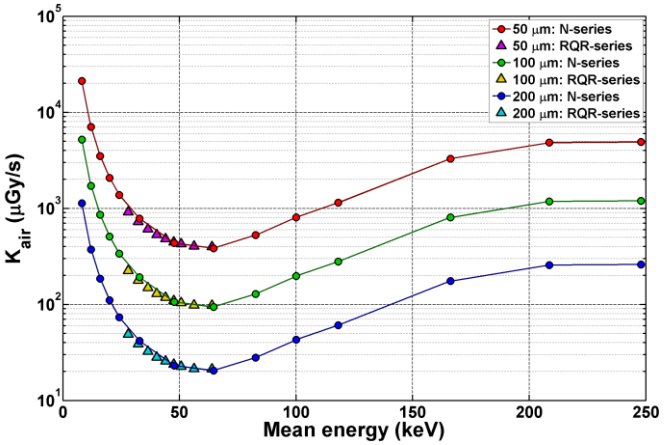

Fig. 16: K_a rate of the X-ray beam as a function of its mean photon energy for CdTe spectrometry measurement when the target detector count rate of 13 000 imp/s is reached with 50 µm, 100 µm, and 200 µm aperture diameter disks used. Data are plotted for N-series (circles) and RQR-series (triangles) qualities.

.

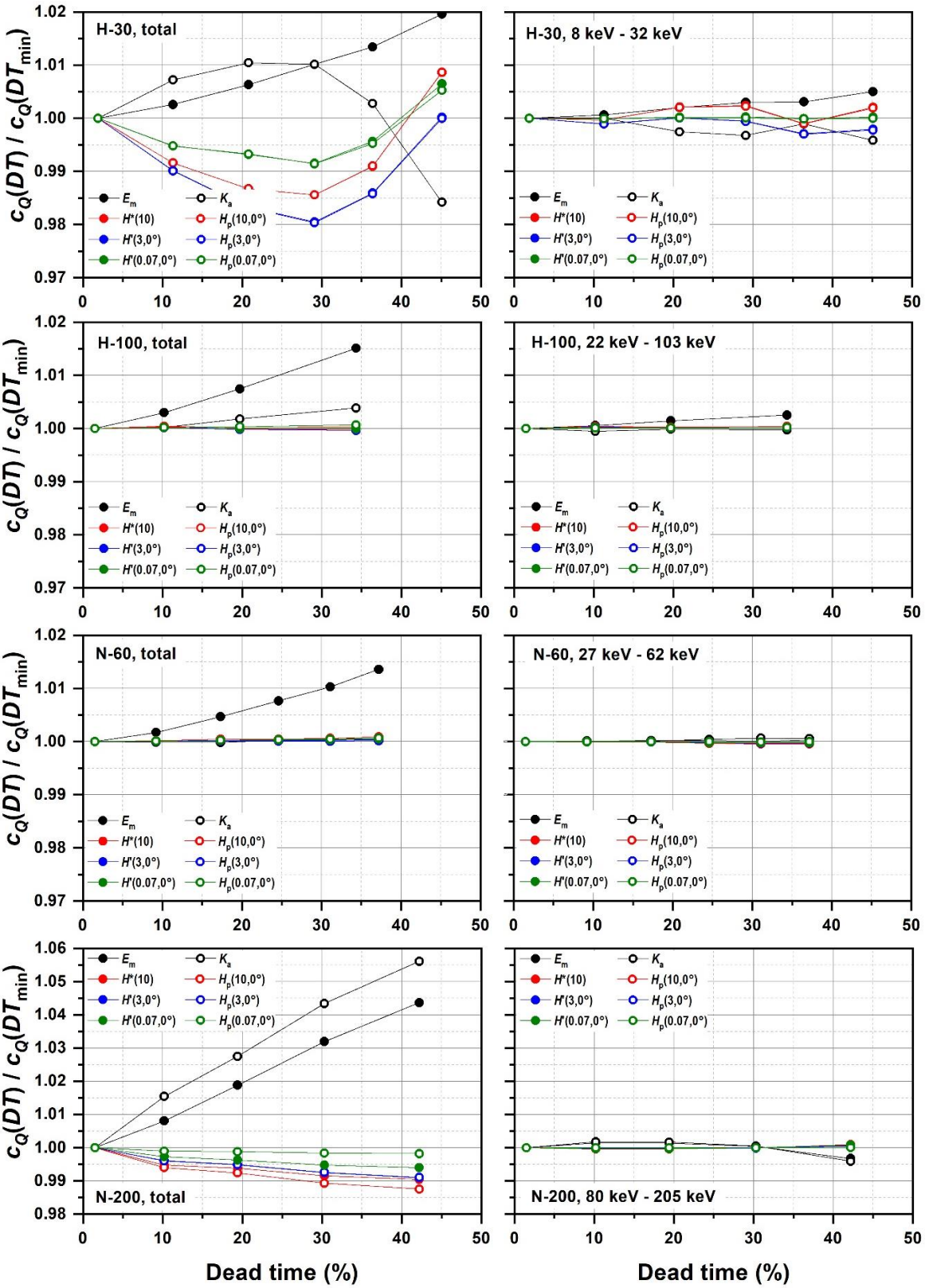

Fig. 17: Selected dosimetric quantities and conversion coefficients derived from unfolded spectra of radiation qualities H-30 (1st row), H-100 (2nd row), N-60 (3rd row) and N-200 (4th row) for different count rates (i.e. different dead times) normalised to the value obtained for a dead time of 2%. The plots show quantities and coefficients calculated for the total spectral range (left) and for the spectral range restricted to photon energies of significant intensity (right) as indicated. Note the different ranges of the ordinates.

For the whole range of dead times investigated with Ge-detector, the dosimetric quantities and conversion coefficients (Fig. 17) derived from unfolded spectra show for H-100 and N-60 a deviation of less than 2 % from the value obtained for a dead time of 2 % when calculated for the total spectral range.

Restricting the spectral range to photon energies of significant intensity and up to the maximum photon energy of the radiation field (see also section 4.3) reduces these deviations to less than 0.5%. For H-30 and N-200 the corresponding quantities and coefficients differ by less than ±2% (H-30) and +6% and −1.5% (N-200) from the value obtained for a dead time of 2% when calculated for the total spectral range. Restricting the spectral range to relevant photon energies reduces the deviations to less than ±0.5%.

Pile-up affects the unfolded spectra in two different ways:

- Appearance of additional structures in the range above the maximum photon energy of the primary radiation field,
- Deterioration of structures present in the photon spectra.

In many cases the count rate has only a minor effect on the derived dosimetric quantities and conversion coefficients: the deviation of the corresponding quantities and coefficients from the value obtained for a dead time of 2% is, except for mean energy, well below 2% when calculated for the total spectral range. However, restricting the spectral range to photon energies of significant intensity and up to the maximum photon energy of the radiation field reduces these deviations substantially and is therefore recommended in the processing of the unfolded spectra. Moreover, a count rate resulting in a dead time as low as possible, as least below 15% is recommended to obtain photon spectra of solid quality with a Ge-detector (for trapezoidally shaped pulses with rise/fall times of 5.6 µs and flat-top time of 1.2 µs). If available, pile-up rejection circuits might prove useful to improve the measured pulse height spectra. The X-123CdTe detector has the pile-up rejection option. Also, in a limited way, pile-up counts can be re-sampled back into the original spectrum during spectrum processing [3].

3.4 Energy calibration of the detector

Due to drift effects in the detector and its electronics and in the electronics of the data acquisition system, the amplification of the system may change, and its zero offset may shift during a spectrometry campaign. Therefore, the energy calibration of the system must be checked periodically using radio nuclide sources. The emission lines of the nuclide sources should cover the energy range of the X-ray fields, which are to be investigated by spectrometry, and should have a high emission probability in this range. A well-suited radio nuclide is ^{133}Ba, which shows several intense emission lines in the range between 30 keV and 400 keV. Another well suited nuclide is ^{57}Co with gamma peaks at 14.4 keV, 122.1 keV and 136.5 keV or ^{152}Eu (121.8 keV, 344.3 keV, 778.9 keV, 964.1 keV, 1408 keV) and ^{137}Cs (661 keV) in case higher energies are needed. The frequency of checking the energy calibration of the system depends on the devices used in the respective system and must be determined individually for each system. In any case it is recommended to carry out a calibration at least before and after a measurement campaign and after detector transport.

Energy calibration of the X-123CdTe detector is described in [2]. Energy calibration is quite stable if the detector settings and environmental conditions are kept constant. The following should be considered, especially when the spectrometer is used for determination of the spectrum end-point energy [2], i.e., non-invasive measurement of high voltage on the X-ray tube:

- Perform the calibration at the total count rate corresponding to the previously fixed count rate for X-ray spectra measurements; this may require using radionuclides with high activity (higher MBq); whenever possible, perform calibration with an attached tungsten collimation disk (responses of the sensor irradiated on the whole area and in the centre only can be different).
- Perform the calibration at the same temperature of the CdTe sensor as reached during X-ray spectra measurements (within ±1 K); this may require a simple external cooling of the shielding around the sensor, e.g., using a computer fan.
- Perform the calibration with radionuclide sources emitting mainly photons with energies corresponding to the X-ray spectra energy range and providing the dead time and count rate corresponding to those achieved in X-ray spectra measurements; as presented in Fig. 15, suitable common radionuclides are ^{133}Ba (30.97 keV, 81.0 keV, 160.6 keV, 223.24 keV, 302.85 keV), ^{57}Co (122.06 keV, 136.47 keV), and ^{241}Am (13.94 keV, 26.35 keV, 59.54 keV), but not ^{152}Eu.

3.5 Shielding against scattered radiation

The use of a suitable shielding against scattered radiation is not mandatory but strongly recommended. Ge-detectors have larger dimensions, resulting in necessary shielding of significant weight. In contrast, handheld CdTe spectrometers enable the design of compact shielding that is easy to manipulate and transport.

Contribution of scattered radiation into the pulse height spectrum can be reduced using:

- Suitable shielding, when possible, around the detector, also from the back,
- A narrow X-ray beam instead of a wide beam,
- A collimation disk with a larger aperture,
- A detector connected with electronics with a long cable Fig. 18, which allows the box with electronics to be removed outside the beam and does not generate scattered photons.

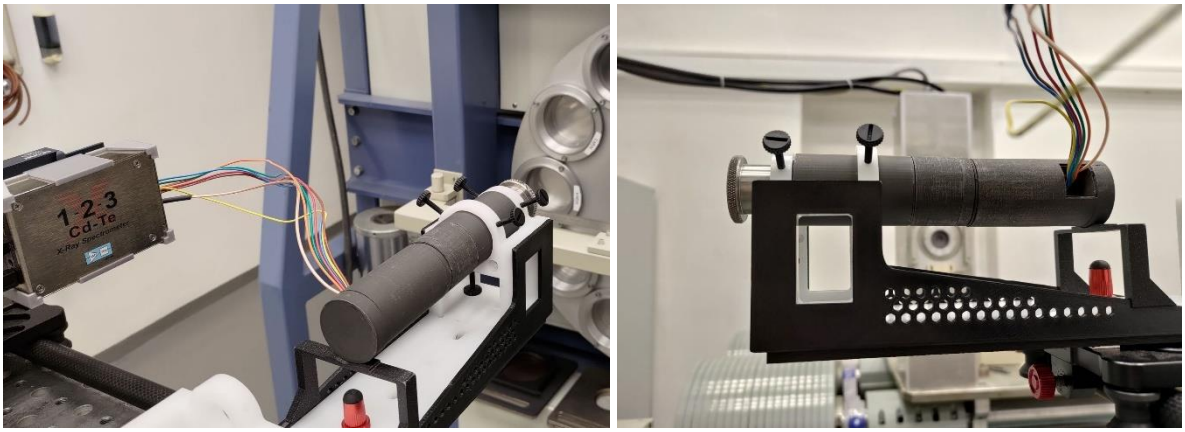

Fig. 18: Shielding for a CdTe detector detached from the electronics and connected with it using a cable.

X-123CdTe detector manufacturer offers a steel collimator (Fig. 2, left), which can provide shielding against scattered radiation for X-ray spectra with the tube voltage up to about ~75 kV.

Measurement of spectra generated with the higher tube voltage requires additional shielding (Fig. 2, right; Fig. 18). The general recommendations for shielding design are as follows:

- Put an effort to remove all unwanted effects physically, rather than to apply corrections to artefacts in measured spectra.
- Use following front shielding:
    - For spectra up to 150 keV: 6 mm of tungsten or equivalent; with this thickness, one 150 keV photon passes through the tungsten material per ~10^6 photons of the same energy passing through the aperture of 3 mm diameter,
    - For spectra with the maximum energy > 150 keV: 6 mm of tungsten + 30 mm of lead or equivalent; with this thickness, the theoretical ratio of the number of 300 keV photons passing through the apertures and through the material of both front shielding is ~7000:1,
    - The diameter should be at least equal to the diameter of the lateral shielding; this allows for elimination of primary photons, which might potentially scatter in the collimator body,
    - Must include an aperture; it serves as the first level of beam collimation before further collimation is achieved using the removable tungsten collimation disks with various aperture diameters,
    - The aperture shape must be perfect, with smooth walls and the axis exactly parallel to the collimator axis, otherwise artefacts described in section 3.2 may occur; this may require a mechanically processed component; also, the aperture area should be known precisely for the purpose of Monte Carlo modelling.
- Use following lateral and rear shielding:
    - Must be shielded against primary photons by front shielding,
    - 5 mm of lead or equivalent,
    - This prevents photons scattered on nearby objects from entering inwards the steel collimator.
- Shielding material with the high proton number (Z) should be put on top of the steel collimator or other lower-Z material:
    - This will ensure that characteristic photons from high-Z shielding material will be attenuated by the lower-Z material sufficiently and do not reach the sensor.
    - This is valid also for positioning of collimation disks; they should be placed far from the sensor.
- The 3D printing technique can be utilised to produce the shielding or its components, especially the lateral and rear shielding, at low costs.

The total weight of the shielding fulfilling the above recommendations and depicted in Fig. 2 is about 0.7 kg (1.3 kg with an external front collimator for beams with the maximum energy > 150 keV).

An example of the extent of the contribution of scattered radiation to the pulse height spectrum of N-150 and RQR10 radiation qualities (both 150 kV tube voltage) acquired with a CdTe detector enclosed in the described shielding with collimation disks with various aperture diameters is presented in Fig. 19.

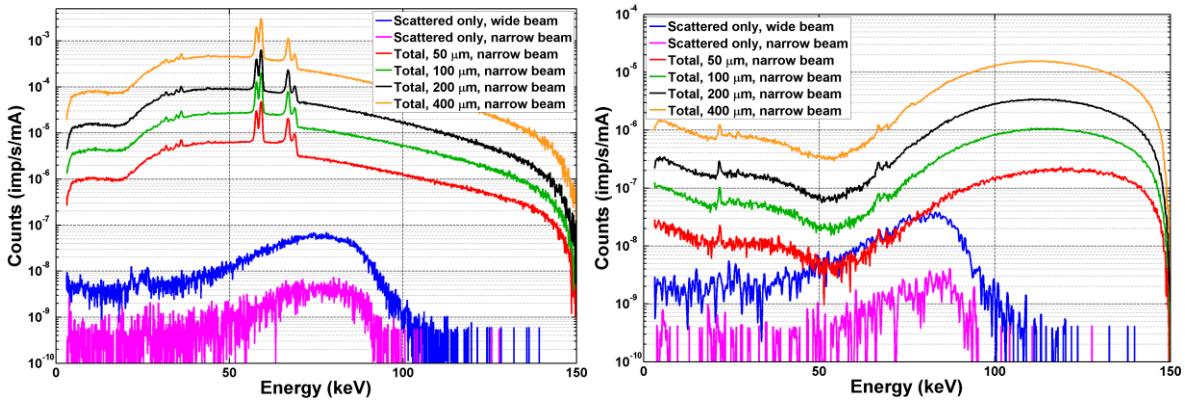

Fig. 19: RQR10 (left) and N-150 (right) spectra measured with a shielded CdTe detector with various aperture diameter collimation disks and with a blocked primary beam (blue and violet). The narrow beam was achieved with a diaphragm restricting the beam diameter to 5 cm at the measurement position while the wide beam was accomplished with the diaphragm removed.

3.6 Cosmic and terrestrial background radiation

The acquired pulse height spectra are affected by cosmic and terrestrial background radiation. However, due to the radiation shield surrounding the detector, and the high fluence from the X-ray tube, the effect of this background radiation generally should not be an issue. For a Ge-detector, Fig. 20 shows a comparison of the count rates of measured pulse height spectra of two radiation qualities of the N-series (N-60 and N-200) and a pulse height spectrum of the cosmic and terrestrial background radiation at the X-ray facility recorded in the same setup, i.e. with radiation shield and entrance aperture/collimator, as the two spectra of the N-series.

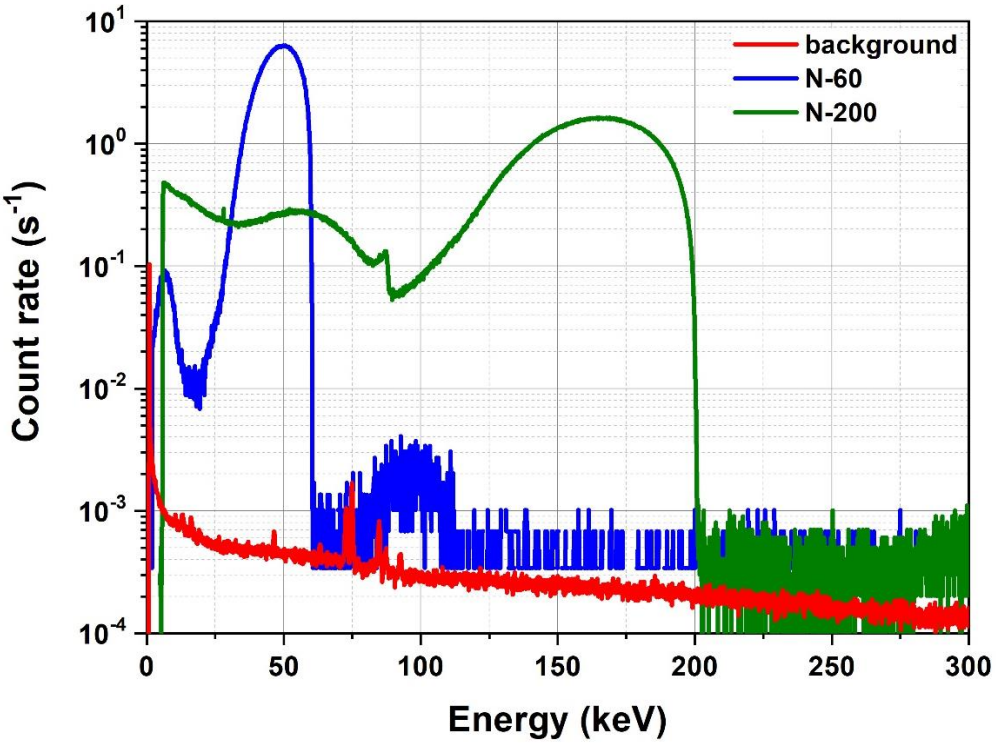

Fig. 20: Count rates of measured pulse height spectra of two radiation qualities of the N-series and a pulse height spectrum of the cosmic and terrestrial background radiation at the X-ray facility measured with a Ge-detector.

The spectra in Fig. 20 clearly show that the background radiation is by several orders of magnitude less intense than the radiation produced by the radiation facility. Nevertheless, it is regarded as good practice to subtract the pulse height spectrum of the background from the pulse height spectrum of the radiation field produced by the X-ray facility. Of course, the background spectrum must be scaled properly by taking into account the ratio of the live times of the two pulse height spectra. In any case recording a background spectrum for the respective X-ray facility is strongly emphasised to allow for an estimation of the contribution of the background radiation.

In the setup with a CdTe detector, the influence of the cosmic and terrestrial background is negligible, because the sensor is very small, it is shielded from all sides, and usually the acquisition time is short.

3.7 Charge carrier transport in CdTe detectors

An intrinsic drawback property of CdTe detectors is the pronounced effect of incomplete charge collection, which is the result of the short lifetime of the holes caused by the density of trapping sites in the crystal. In the pulse height spectra, this effect is expressed in asymmetric full-energy peaks extending towards lower energies (Fig. 21). This also results in a small shift of the peak maximum to lower energies. The peak shift is important when the goal of the spectrometry is to determine the energy distribution of primary photon fluence. Therefore, when the pulse height spectrum is used in a procedure aiming to determine the primary photon fluence spectrum, the charge carrier transport (CCT) properties in CdTe should be considered.

CCT physical models can be applied either on the pulse height spectrum or on the Monte Carlo simulated detector responses. The latter option is described in [4]. Neglecting the CCT in the unfolding of fluence spectra leads to systematic deviations in quantities calculated from the fluence spectra. The extent heavily varies depending on the radiation quality and the calculated quantity. For selected qualities and quantities, analysis was performed in [2].

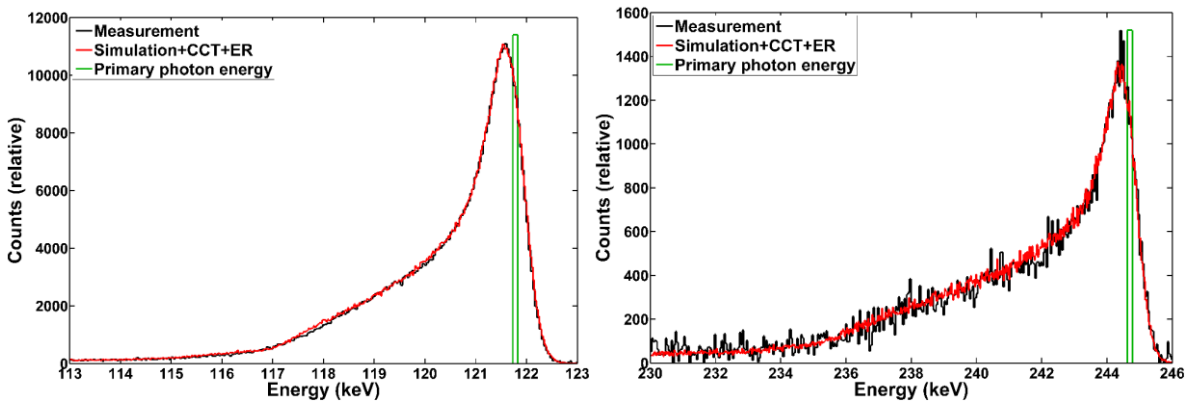

Fig. 21: Comparison of simulated (red) and measured (black) full-energy peaks at 121.8 keV and 244.7 keV (^{152}Eu) measured with a CdTe detector. The charge carrier transport (CCT) model and energy resolution (ER) were applied on simulated data.

3.8 Pulse shape timing parameters

The output pulses of the charge sensitive preamplifier incorporated inside the housing of the Ge-detector are shaped trapezoidally by the digital pulse processor, with defined rise (fall) time of the rising (falling) edge and flat-top time of the trapezoid, where rise time and fall time are identical. Both, rise/fall time and fat top time, affect the total pulse length of the trapezoid and

with it the system's dead time: the shorter the pulse length, the lower the dead time for a given count rate. However, the pulse length of the trapezoid in turn affects the energy resolution and the correspondence between photon energy and channel number, i.e. the energy calibration, of the measured pulse height spectrum. Fig. 22 shows the effect of pulse shape timing parameters on FWHM and shift of the emission lines of a ^{133}Ba nuclide source. The shift of the emission lines is determined relative to the optimized second order fitting polynomial for the reference setting of a rise/fall time of 5.6 µs and a flat-top time of 1.2 µs.

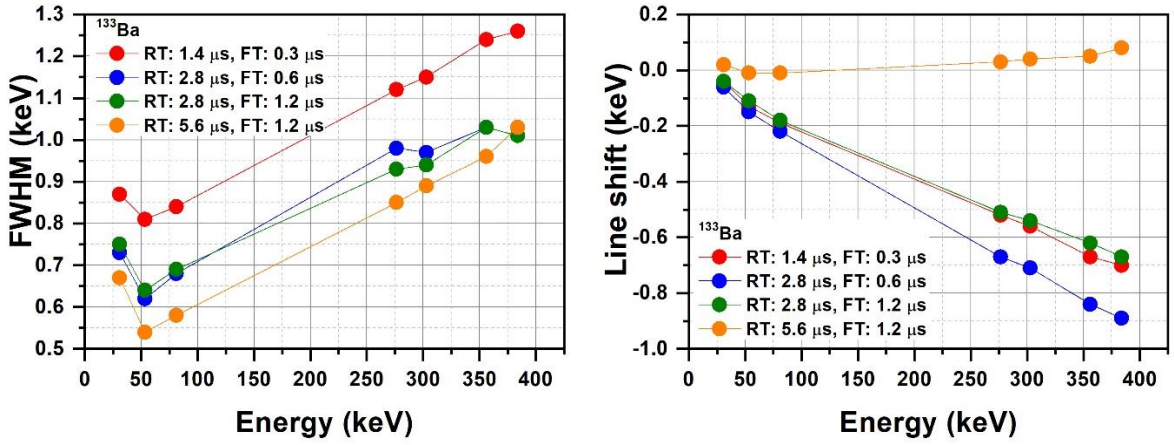

Fig. 22: FWHM (left) and shift of the emission lines (right) in pulse height spectra of a ^{133}Ba nuclide source for different combinations of rise/fall times (RT) and flat top times (FT) of the trapezoidally shaped pulse. The reference setting is the combination of a rise/fall time of 5.6 µs and a flat top time of 1.2 µs, which corresponds to the default setting of the digital pulse processor.

The FWHM increases with decreasing pulse length. The FWHM of the different combinations of rise/fall time and flat-top time are shifted almost parallel, i.e. the amount of the increase is almost independent from the photon energy. However, the FWHM for the two combinations with rise/fall time of 2.8 µs and flat-top time of 1.2 µs and with rise/fall time of 2.8 µs and flat-top time of 0.6 µs, respectively, differ only slightly, indicating that the rise/fall time is the dominating factor for the increase of the FWHM.

For the shift of the emission lines no clear dependency on the pulse length is observed, as the coinciding FWHM for the two combinations with rise/fall time of 2.8 µs and flat-top time of 0.6 µs and with rise/fall time of 1.4 µs and flat-top time of 0.3 µs, respectively, indicate. Nevertheless, the emission lines tend to shift towards lower channel numbers in the pulse height spectra which transforms into a shift towards lower photon energies, when calibrating the energy of the pulse height spectrum by applying the optimised second order fitting polynomial for the reference setting of a rise/fall time of 5.6 µs and a flat top time of 1.2 µs. Consequently, changing the rise/fall time and/or the flat-top time requires a new energy calibration of the pulse height spectrum.

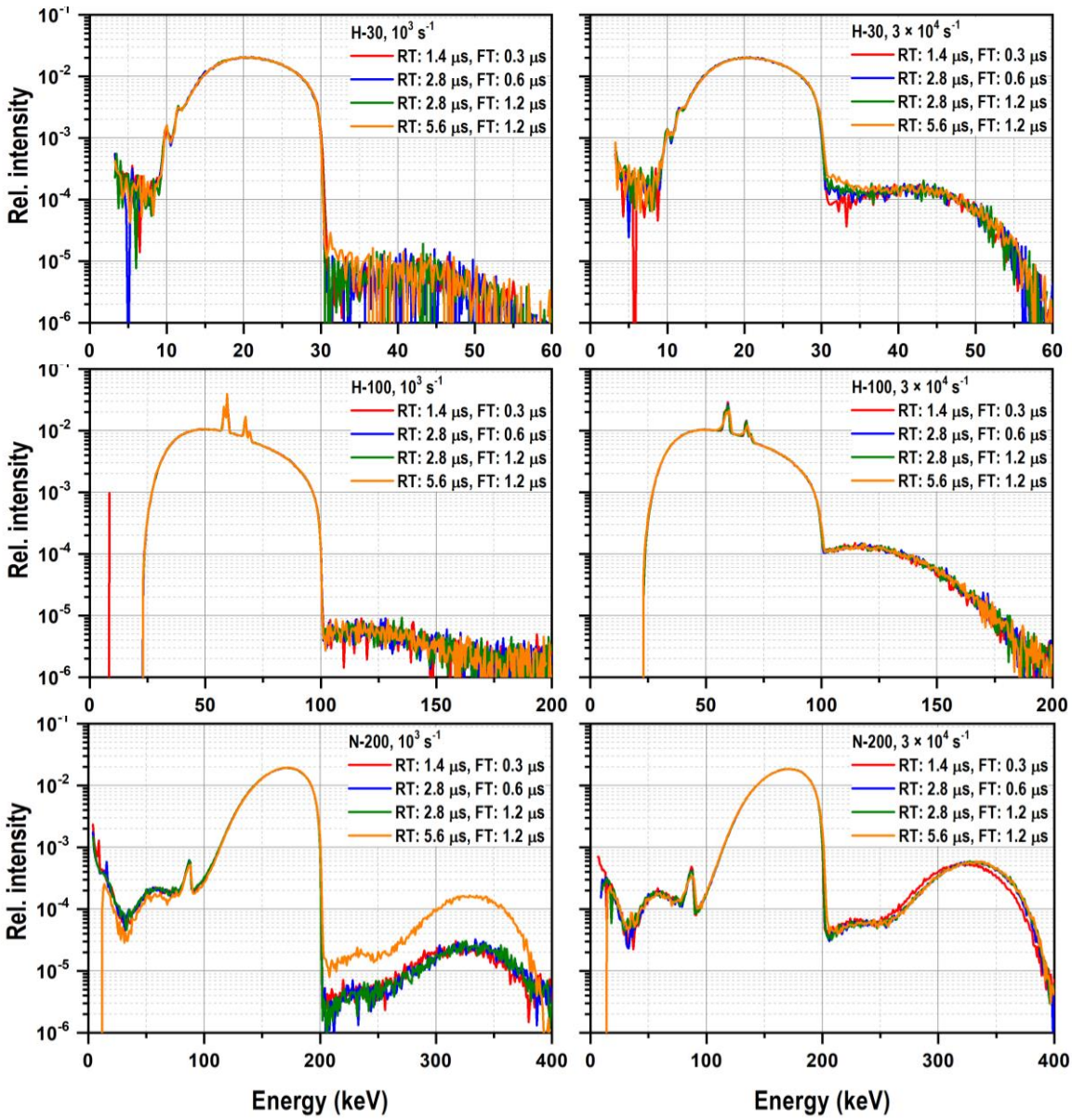

Fig. 23: Unfolded photon fluence spectra of radiation qualities H-30 (1st row), H-100 (2nd row) and N-200 (3rd row) for count rates of 10^3 s^{-1} (left) and 3×10^4 s^{-1} (right) measured with a Ge-detector followed by a digital pulse processor using different combinations of rise/fall time (RT) and flat top time (FT) for the trapezoidally shaped pulse.

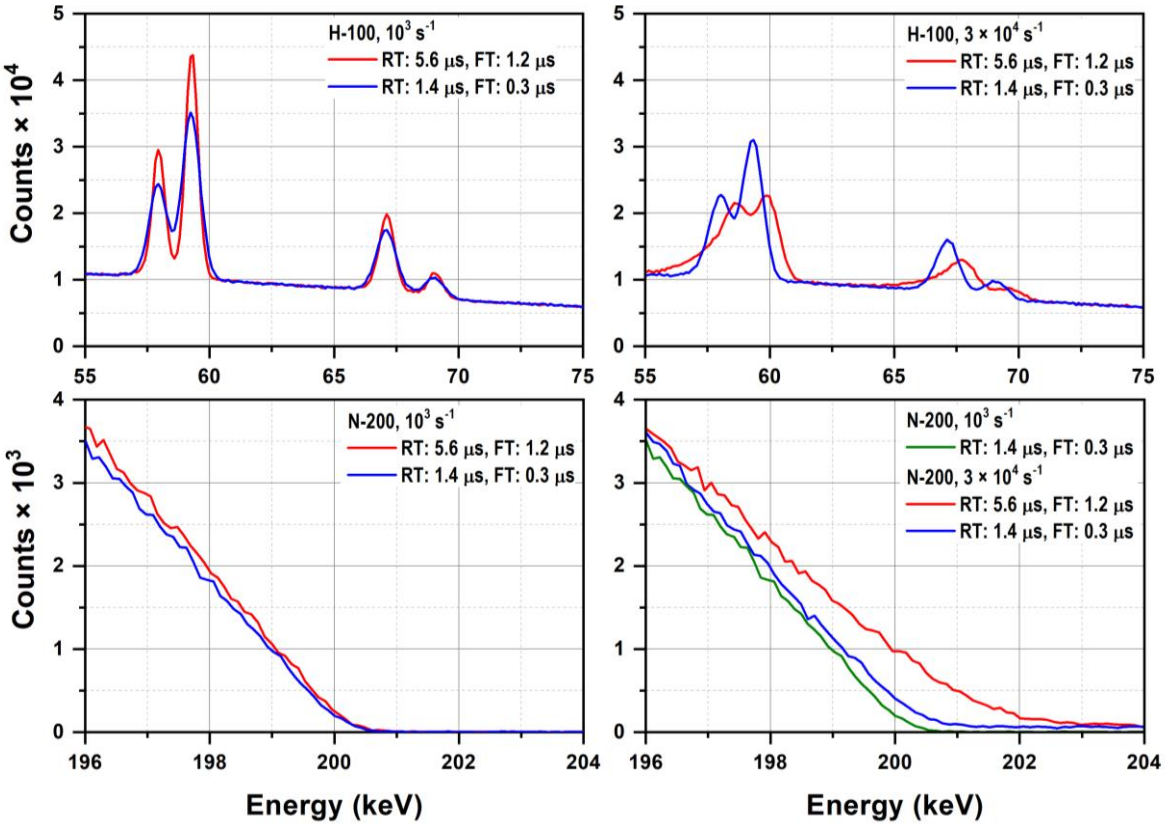

Fig. 24: Details of the pulse height spectra of H-100 (top row) and N-200 (bottom row) for count rates of 10^3 s^{-1} and 3×10^4 s^{-1} and combinations of rise/fall time (RT) and flat top time (FT) with rise/fall time of 5.6 µs and flat top time of 1.2 µs and with rise/fall time of 1.4 µs and flat top time of 0.3 µs, respectively, for the trapezoidally shaped pulse.

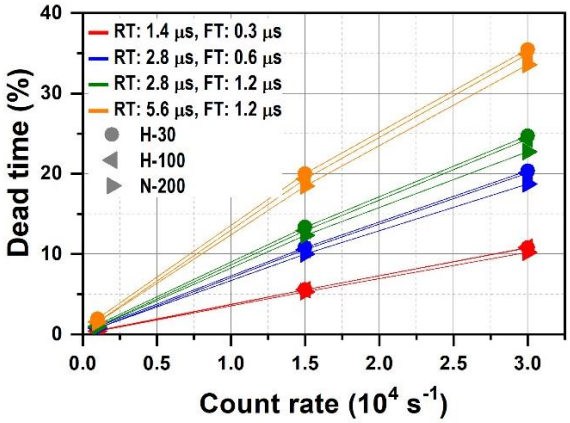

Fig. 25: Dead time in dependence on the count rate for selected radiation qualities for trapezoidally shaped pulses with different combinations of rise/fall time (RT) and flat-top time (FT).

Fig. 23 shows the effect of different combinations of rise/fall time and flat-top time on the unfolded spectra of different radiation qualities for different count rates. Although the dead time decreases with decreasing length of the trapezoidally shaped pulses, no effect of the pulse length is observed on the unfolded spectra, in particular not in the energy range where pile-up is up to occur due to high count rates. To some extent, this behaviour can be expected for low count rates, where dead times are low, but for high count rates a reduction of pile-up would be expected.

Fig. 24 shows details in the pulse height spectra of H-100 and N-200 for different count rates and combinations of rise/fall time and flat-top time for the trapezoidally shaped pulse. The number of counts is identical in all pulse height spectra of each radiation quality. The plot for H-100 (top row) shows the W fluorescence lines of the X-ray tube's anode. For low count rate (top left), the emission lines are well resolved for both combinations of rise/fall time and flat-top time. However, for long pulses (RT = 5.6 µs and FT = 1.2 µs) a better energy resolution is observed than for short pulses (RT = 1.4 µs and FT = 0.3 µs). For high count rate (top right), deterioration of the energy resolution is observed for both pulse lengths, where the deterioration is significantly more pronounced for long pulses than for short pulses, and the fluorescence lines shift towards higher energies for long pulses (see also Fig. 14).

As already shown in Fig. 14, the pulse height spectrum close to the maximum photon energy of the radiation field, which corresponds to the high voltage applied to the X-ray tube, is increasingly blurred and shifted towards higher energy with increasing count rate, making it harder (or even impossible) to determine the maximum photon energy of the radiation field. The effect of the pulse length on the high energy edge of the radiation quality N-200 is shown in the bottom row of Fig. 24. For low count rate, the pulse height spectra for short and long pulses coincide in the vicinity of the maximum photon energy. For high count rate, no blurring and only a slight shift of the high energy edge is observed for short pulses, whereas for long pulses a substantial blurring and a significant shift of the maximum photon energy is found.

Fig. 25

shows the dead time in dependence on the count rate for selected radiation qualities for trapezoidally shaped pulses with different combinations of rise/fall time and flat-top time. For all radiation qualities and count rates, the dead time decreases with decreasing pulse length.

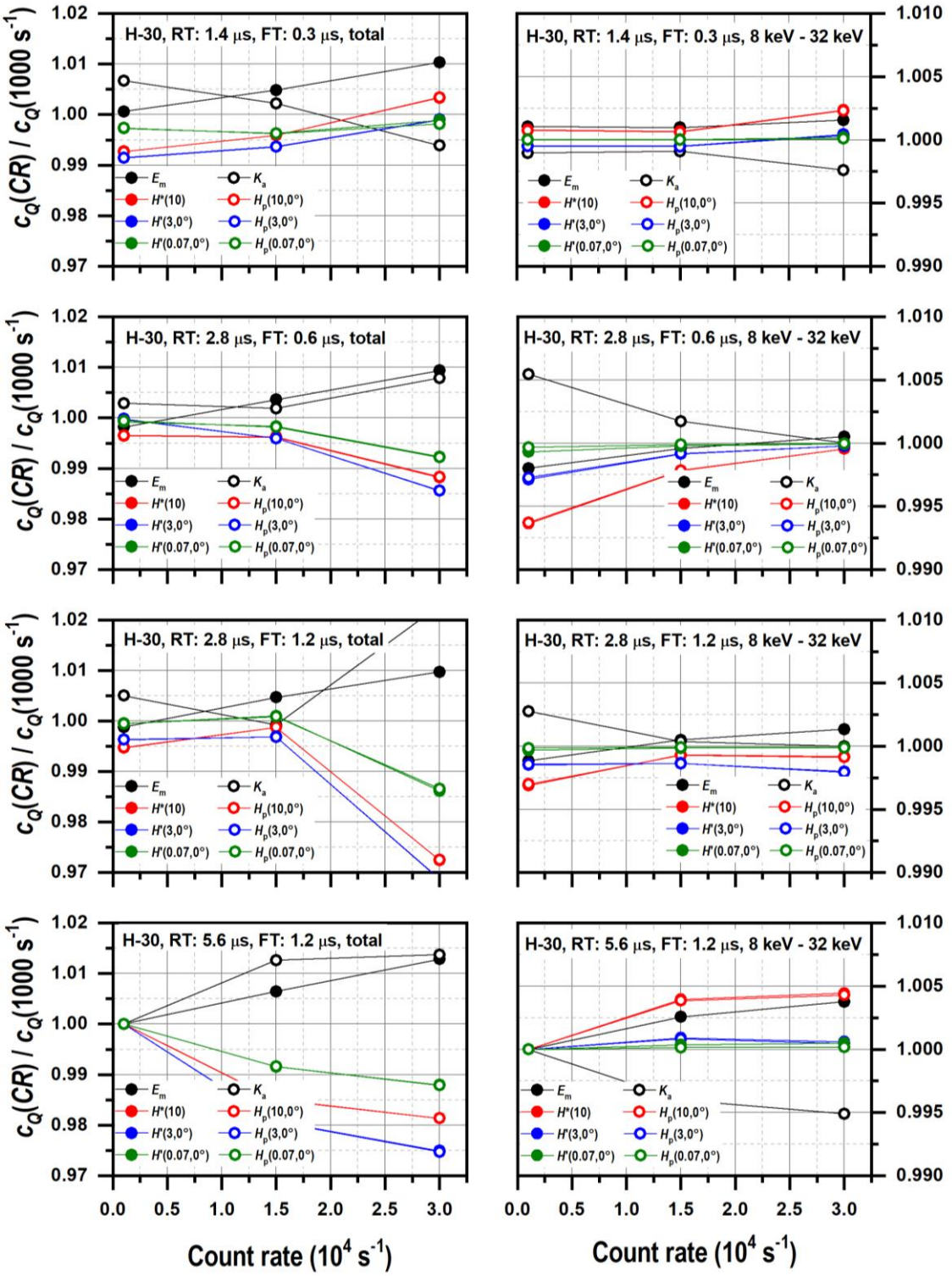

Fig. 26: Selected dosimetric quantities and conversion coefficients derived from unfolded spectra of radiation quality H-30 for different combinations of rise/fall time (RT) and flat top time (FT) (1st row: RT = 1.4 µs, FT = 0.3 µs; 2nd row: RT = 2.8 µs, FT = 0.6 µs; 3rd row: RT = 2.8 µs, FT = 1.2 µs; 4th row: RT = 5.6 µs, FT = 1.2 µs) and different count rates normalised to the value obtained for a count rate of 10^3 s^{-1} and a pulse with RT = 5.6 µs and FT = 1.2 µs. The plots show quantities and coefficients calculated for the total spectral range (left) and for the spectral range restricted to photon energies of significant intensity (right) as indicated. Note the different ranges of the ordinates.

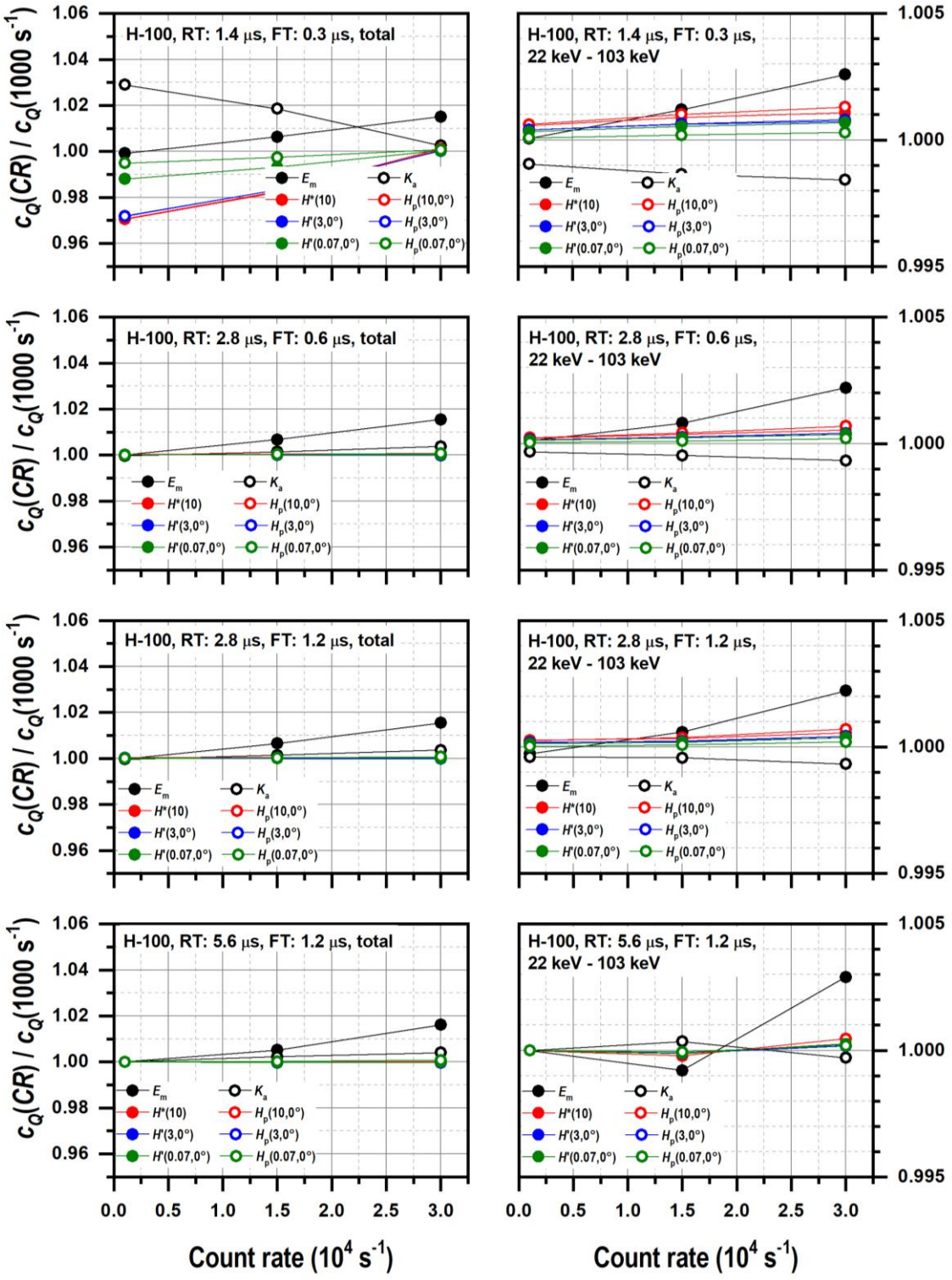

Fig. 27: Selected dosimetric quantities and conversion coefficients derived from unfolded spectra of radiation quality H-100 for different combinations of rise/fall time (RT) and flat top time (FT) (1st row: RT = 1.4 µs, FT = 0.3 µs; 2nd row: RT = 2.8 µs, FT = 0.6 µs; 3rd row: RT = 2.8 µs, FT = 1.2 µs; 4th row: RT = 5.6 µs, FT = 1.2 µs) and different count rates normalised to the value obtained for a count rate of $10^3\ s^{-1}$ and a pulse with RT = 5.6 µs and FT = 1.2 µs. The plots show quantities and coefficients calculated for the total spectral range (left) and for the spectral range restricted to photon energies of significant intensity (right) as indicated. Note the different ranges of the ordinates.

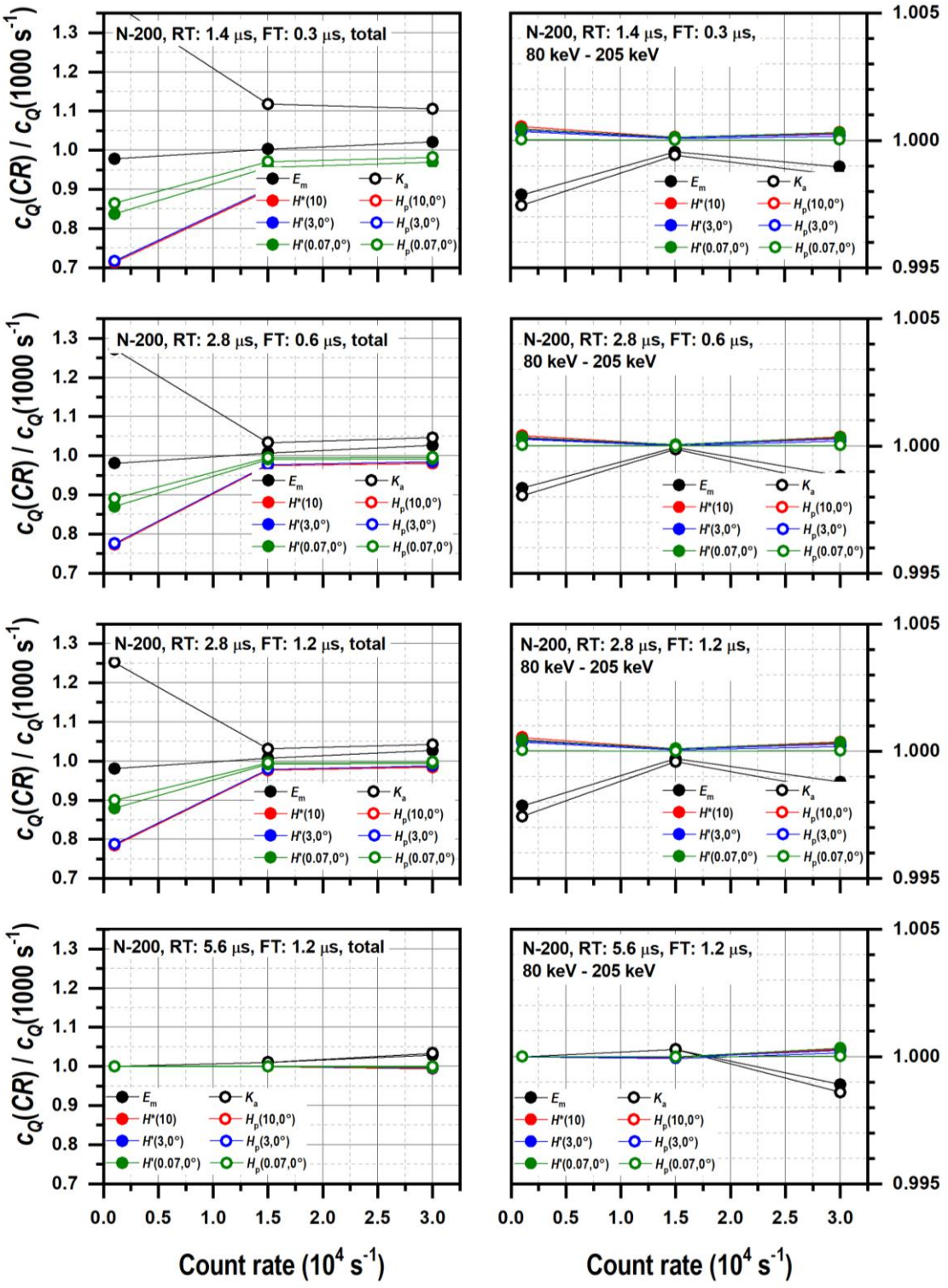

Fig. 28: Selected dosimetric quantities and conversion coefficients derived from unfolded spectra of radiation quality N-200 for different combinations of rise/fall time (RT) and flat top time (FT) (1st row: RT = 1.4 µs, FT = 0.3 µs; 2nd row: RT = 2.8 µs, FT = 0.6 µs; 3rd row: RT = 2.8 µs, FT = 1.2 µs; 4th row: RT = 5.6 µs, FT = 1.2 µs) and different count rates normalised to the value obtained for a count rate of 10^3 s^{-1} and a pulse with RT = 5.6 µs and FT = 1.2 µs. The plots show quantities and coefficients calculated for the total spectral range (left) and for the spectral range restricted to photon energies of significant intensity (right) as indicated. Note the different ranges of the ordinates.

The dosimetric quantities and conversion coefficients derived from unfolded spectra for H-30, H-100 and N-200 are shown in Figs. 26-28. The quantities and coefficients are determined for different combinations of rise/fall time (RT) and flat top time (FT) and different count rates and are normalised to the value obtained for a count rate of 10^3 s^{-1} and a pulse with RT = 5.6 µs and FT = 1.2 µs. Deviations of ±4% for H-30 and H-100 and up to +30% and −25% for N-200 are observed when calculated for the total spectral range. Restricting the spectral range to photon energies of significant intensity and up to the maximum photon energy of the radiation field reduces these deviations to less than ±0.5% for all radiation qualities, all pulse length and all count rates investigated.

For setup with a CdTe detector, such comprehensive analysis has not been carried out. However, from the current experience it is assumed that the CdTe detectors behave in a similar way when changing different pulse-shaping parameters.

The setting presented in [1] was found adequate for a detector with a 3 mm × 3 mm area CdTe sensor:

- Cooler temperature 220 K (or lowest possible), high voltage bias +950 V (maximum possible according to the manual, not recommended to set higher), peaking time 2.4 µs, flat top width 0.6 µs, fast threshold 9.93, fast channel peaking time 100, advanced base time restoration mode 1 (use 3 if available), clock speed 80 MHz, pile-up rejection turned on, and rise time discrimination turned off.

For a CdTe detector with a 5 mm × 5 mm area sensor attached to the electronics with a cable, the following settings were found adequate:

- Cooler temperature 219 K (or lowest possible), high voltage bias +800 V (maximum possible according to the manual, not recommended to set higher), peaking time 2.4 µs, flat top width 1.0 µs, fast threshold 7.50, fast channel peaking time 400, advanced base time restoration mode 3, clock speed 80 MHz, pile-up rejection turned on, and rise time discrimination turned off.

3.9 Statistics of counts in energy bins

Laboratory measurements allow for long acquisition time, ensuring high statistics of counts in individual energy bins. However, some facilities do not provide a possibility for long irradiations. Recommendations for CdTe spectrometry are as follows:

- For a count rate of 13 000 imp/s, at least 60 s of continuous irradiation time, optimally 3-5 min, depending on the energy range of the spectrum,
- A few thousand counts per energy bin in the main part of the spectrum continuum,
- Use smoothing of the pulse height spectrum, e.g., the adaptive-degree Savitzky-Golay algorithm [6].

3.10 Recommended spectrometry settings

From the findings presented in the previous chapters several recommendations, more focused on Ge-detectors, can be obtained:

- The angle of misalignment between the central axis of the collimating aperture and the propagation direction of the photons emitted from the X-ray source should be less than 0.5° for a collimating aperture with diameter and length of 1.13 mm and 60 mm, respectively; for collimating apertures of other dimensions the maximum permissible angle of misalignment will be different.

- Best energy resolution is obtained for long pulses; use long pulses with low count rates resulting in a dead time below 15% to prevent pile-up and energy shifts, whenever possible; if available, pile-up rejection circuits might prove useful to improve the measured pulse height spectra; as in the digital pulse processor used in this investigation pile-up rejection is not available, this aspect was not considered.
- Decrease pulse lengths, whenever low count rates are not achievable; although using short pulses does not reduce pile-up, the energy resolution is preserved better and the energy shift is less compared to long pulses at high count rates.
- Changing the pulse length requires a new energy calibration of the acquisition system.
- Check the energy calibration of the acquisition system periodically, preferably before and after each measurement session.
- Record pulse height spectra of the cosmic and terrestrial background radiation; if necessary, subtract the background spectrum from the measured X-ray spectra.
- Restrict the spectral range to photon energies of significant intensity and up to the maximum photon energy of the radiation field determined by the high voltage applied to the X-ray tube, when determining dosimetric quantities and conversion coefficients from unfolded spectra.

It must be pointed out, that the findings presented in the previous chapters are valid, strictly speaking, only for the acquisition system applied in the present investigation, i.e. a specific Ge-detector and a specific digital pulse processor of a specific manufacturer. While different Ge-detectors can be expected to behave similar under similar conditions, this cannot be expected a priori for different pulse processors. Different pulse processors may use different algorithms for processing like pulse shaping, pile-up correction/suppression, etc., and therefore must be regarded as “black boxes”, where the pulse processing is completely non-transparent for the user. Consequently, the previously mentioned findings are of limited transferability and the resulting conclusions should not be seen as strict rules but rather as recommendations, and moreover, they point out aspects which should be inspected for a given acquisition system.

For systems with CdTe spectrometers X-123CdTe, it can be assumed that these detectors behave similarly when comparing to each other, as the electronics are the same. However, a thorough investigation on settings optimal for high-count rate in-beam X-ray spectrometry in the energy range up to a few hundred keV is still missing.

4. Spectrum unfolding

The characterisation of the X-ray fields is carried out by spectrometry using appropriate radiation detectors. As inside semiconductor detectors different types of interaction processes take place, which themselves have cross sections of different energy dependence, the response of the detectors depends significantly on the photon energy of the incident photons. Consequently, the measured pulse height spectrum is deformed with respect to the incoming “true” X-ray spectrum. The “true” spectrum can be obtained from the measured pulse height spectrum using a suitable unfolding procedure, which requires the determination of the detector’s energy dependent response. Mathematically, the detector response has matrix form and is obtained by Monte Carlo simulations, which require a geometry model of the setup of the detecting crystal and its complete surrounding reflecting the real setup as close as possible, and by measurements supporting the simulations.

Unfolding of photon fluence spectra measured with a CdTe detector follows the same path and it is detailed in [1] and [4].

4.1 The detector response matrix

The detector response matrix is obtained using Monte Carlo simulations. The MC model must include all components of the measurement geometry that have any influence on the pulse height spectrum. This includes a sensor with contacts and dead layers, geometry just behind the sensor contributing to direct backscatter, an entrance window, front collimation with an accurate model of the aperture, and at least the inner components of the collimator/shielding to take into account scattering inside the collimation system. The area of the planar monoenergetic photon source must cover all components potentially influencing the pulse height spectrum. Therefore, if the shielding is not sufficient, the source area should be much larger, which significantly decreases the efficiency of MC simulations.

Fig. 29 and Fig. 30 show response matrices of Ge and CdTe detectors, respectively. In Fig. 29 the energy dependent response functions to monoenergetic incident photons, folded with the energy resolution of a detector, are indicated by the black lines parallel to the x-axis. On the y-axis the energy of the photon incident on the Ge-detector is plotted. The x-axis corresponds to energy recorded in the respective pulse height spectrum. The z-axis represents the probability to record (detect) an energy deposition of defined energy in the pulse height spectrum for an incident photon of specified energy.

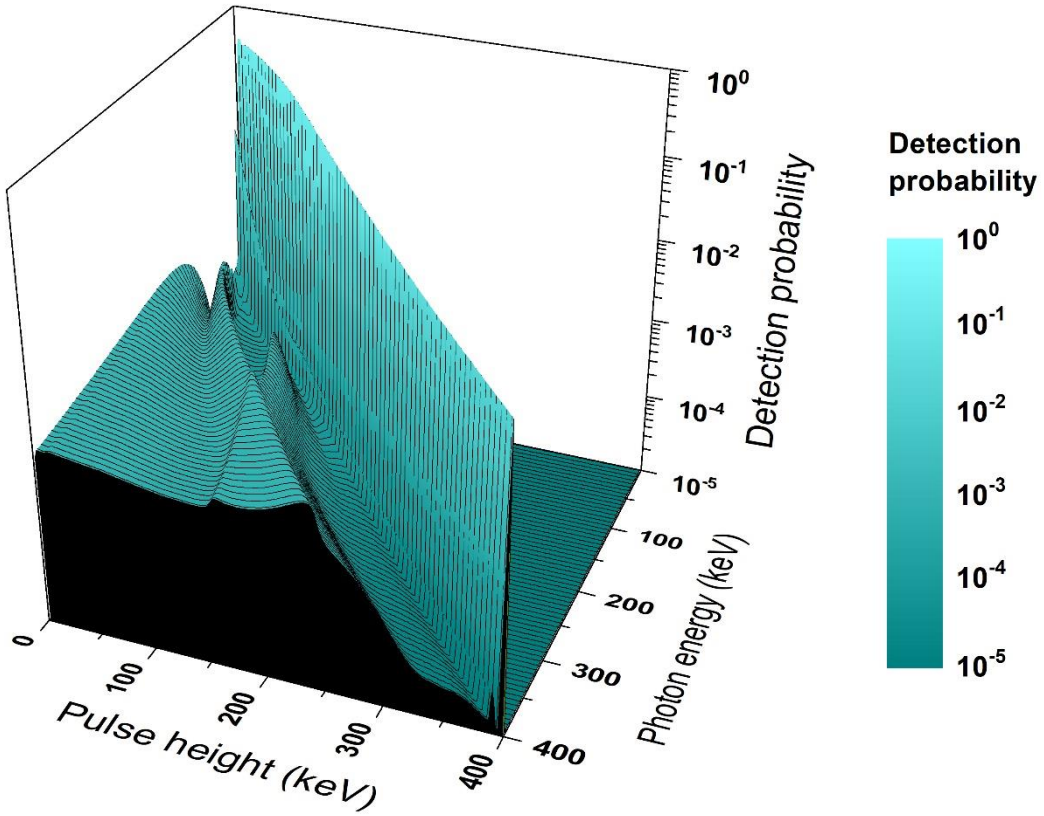

Fig. 29: 3D plot of a response matrix covering the energy range 0 – 400 keV. Y-axis: energy of the photon incident on the Ge-detector; x-axis: energy recorded in the corresponding pulse height spectrum; z-axis: probability to record (detect) an energy deposition of defined energy in the pulse height spectrum for an incident photon of specified energy.

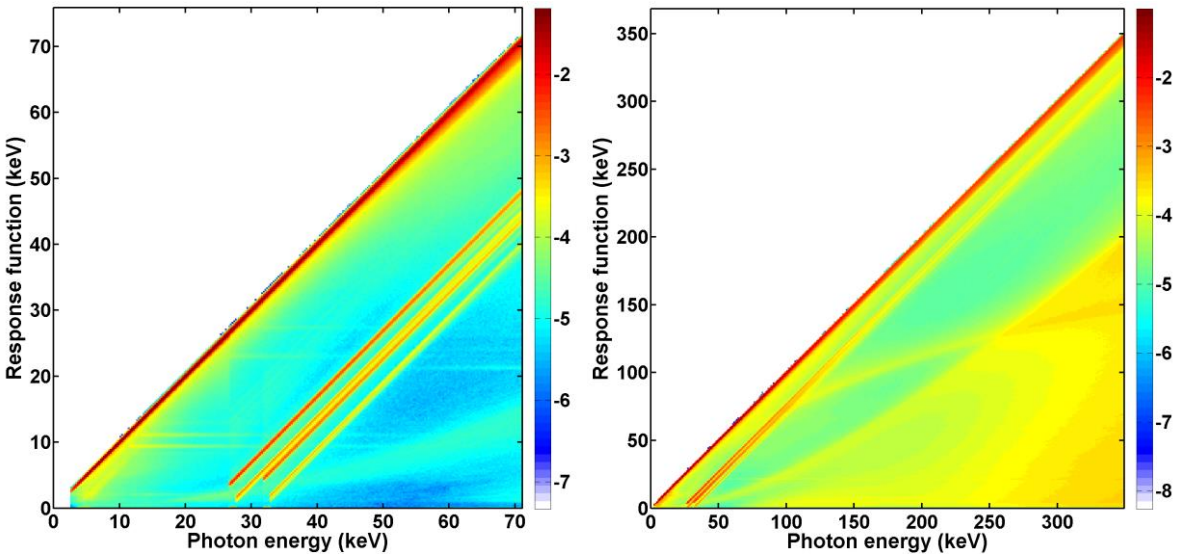

Fig. 30: Response matrices of X-123CdTe spectrometer in the energy range up to 70 keV (left) and up to 350 keV (right). X-axis: energy of the incident photon; y-axis: energy recorded in the corresponding pulse height spectrum; colour axis: relative number of counts of given energy.

Depending on the total range of photon energies to be covered, it should be considered to split the response into several matrices, especially if the required energy resolution de~~in~~creases with photon energy. This limits the matrix rank and speeds up the unfolding (depending on the unfolding procedure). For example, the photon energy range of 0 – 400 keV may be split into four matrices of identical rank, one with 0 – 40 keV and 0.1 keV resolution, the second with 0 – 100 keV and 0.25 keV resolution, the third with 0 – 200 keV and 0.5 keV resolution and the fourth with 0 – 400 keV and 1 keV resolution. The maximum energy of the matrices should be slightly larger than the maximum energy in the intended range of use to allow for unfolding those pulse height spectra with maximum energy at the upper limit of the respective range of use, i.e. the matrix covering the intended range of use of 0 – 100 keV should extend to slightly larger energy, e.g. to 105 keV, to allow for unfolding of pulse height spectra produced with operating voltages of the X-ray tube of 100 kV.

An example of another choice of energy binning and energy ranges of response matrices for a CdTe spectrometer is shown in Table 1.

Table 1: The number of response functions for each set of collimation disks and the energy steps.

Extension front lead collimator(1)	no	no	yes	yes
Primary photon energy	2.5 – 27.0 keV	27 – 155 keV	140 – 155 keV	155 – 311 keV
Number of response functions	196	512	60	156
Response function energy step, response matrix bin width, unfolded spectrum bin width	0.125 keV	0.25 keV	0.25 keV	1.0 keV

(1) Additional front shielding and collimation used only for measurement of spectra with E > 150 keV.

4.2 Unfolding procedure

The “true” photon spectrum can be obtained from the measured pulse height spectrum using a suitable unfolding procedure. For this purpose, an iterative unfolding algorithm using Bayes

statistics as described in [7] and [8] can be employed. The iteration formula (iteration n) of this algorithm is:

$$\Phi_{U_i}^{n+1} = \frac{\Phi_{U_i}^{n}}{\sum_k R_{k,i}} \cdot \sum_k \frac{R_{k,i} \cdot \Phi_{M_i}}{\sum_j R_{k,j} \cdot \Phi_{U_j}^{n}}$$

with: Φ_U: unfolded photon spectrum

Φ_M: measured pulse height spectrum

R: detector response matrix

i, j, k: matrix/spectrum indices

Besides the response matrix and the measured pulse height spectrum, an initial estimate $\Phi_{U_i}^{0}$ must be provided by the user, e.g. a uniform distribution of counts normalised to an integral of unity:

$$\Phi_{U_i}^{0} = \frac{1}{i_{max}} \qquad \text{for: } 1 \leq i \leq i_{max}$$

where i_{max} denotes the rank of the detector response matrix. Normalisation of the measured pulse height spectrum with respect to an integral of unity should be considered, since by this normalisation a probability distribution is achieved reflecting the probability of energy deposition in the detector per incident photon of the X-ray radiation field. The result of the unfolding procedure is then also normalised to an integral of unity (except for rounding errors) representing the probability distribution of the photon energies in the radiation field per incident photon.

Alternatively, various toolkits based on other iterative algorithms are available, for example, an implementation of the maximum likelihood estimation using expectation maximisation available with a graphical interface [9] or the software GRAVEL [10]. Non-iterative unfolding methods are the stripping method, escape peak correction algorithm, least-squares methods or the maximum entropy principles.

Additionally, it is worthwhile to fold back the unfolding of the measured spectrum with the detector's response matrix. The result of this procedure should closely approximate the measured pulse height spectrum.

Fig. 31 shows and example of the unfolding of a pulse height spectrum measured with a Ge-detector for the N-300 X-ray radiation quality together with the subsequently back folding of the unfolding. Similarly, Fig. 32 presents measured and unfolded spectra obtained with a CdTe spectrometer.

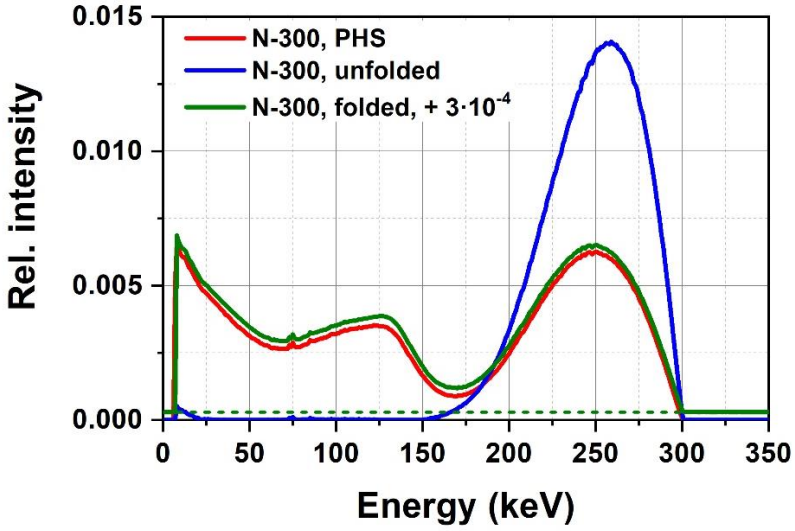

Fig. 31: Measured pulse height spectrum (red) and corresponding unfolding (blue) for spectrum N-300 of the narrow spectrum series. The unfolding is folded back with the response matrix (green) and is shifted towards higher values by $3 \cdot 10^{-4}$ for better clarity of view. The dashed green line represents the zero line for the back folded unfolding.

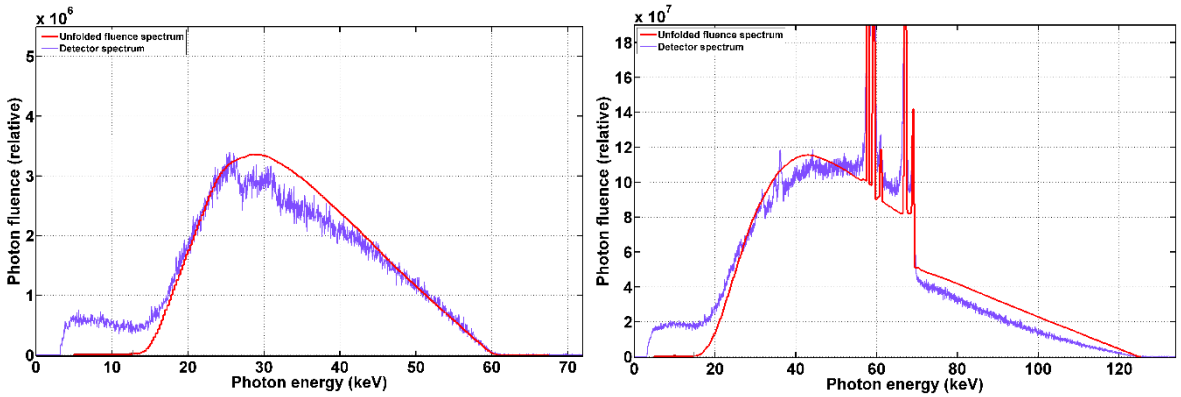

Fig. 32: Examples of X-ray spectra measured with a CdTe detector (blue) and the corresponding unfolded primary photon fluence spectra (red). Left - 60 kV tube voltage; right - 125 kV tube voltage.

4.3 Trimming of unfolded fluence spectra

The energy range of the unfolded spectra extends over the whole energy range covered by the detector response matrix and is, therefore, in general larger than the energy range of the photons of the X-ray radiation field. Hence, it is justified to trim the unfolded spectra such that only intensities in the relevant energy range are preserved, i.e. setting intensities to zero slightly above the X-ray tube's operation voltage and slightly below the low energy cutoff caused by the filtering. Trimming the unfolded spectra in this way prevents effects of noise in the energy ranges outside the photon spectrum, caused by the unfolding procedure, on the determination of various characteristics of the respective X-ray radiation field like mean photon energy, kerma factor or conversion coefficients for radiation protection quantities.

Noise and artefacts caused by unfolding cannot be fully avoided. Firstly, the Monte Carlo model used to calculate the response matrix never covers all effects that occur in measurements, whatever the reason is (e.g., simplified geometry, improper detector alignment, proprietary information on detector components, neglected influence of backscatter, cross-section table uncertainty, simplification of interaction modelling, neglected or simplified modelling of

incomplete charge collection, etc.). Secondly, the measured spectrum always has some statistics on the registered number of counts per channel. That is why the trimming of unfolded spectra is reasonable and, in most cases, also necessary. However, the user has to be careful and perform the trimming on a spectrum-to-spectrum basis, namely, to avoid unwanted removal of low-energy characteristic peaks occurring in some X-ray spectra.

5. Uncertainty of the spectrometry method

Each spectrometry setup is different, and therefore, each uncertainty must be evaluated individually. The uncertainty budget with examples for uncertainty contributions of GuideRadPROS project partners in the Appendix 8.1 can serve as a first guidance.

6. Conclusions

The aim of this document was to summarise recommendations and provide guidance on procedures and experimental setup for spectrometry of reference X-ray radiation fields in laboratories utilising traditional germanium spectrometers and compact cadmium telluride detectors.

7. References

[1] J. Šolc, J. Šmoldasová, L. Štemberková, V. Sochor, Z. Vykydal. Improved setup and characterization of cadmium telluride detector for in-beam X-ray spectrometry up to 300 kV at Czech Metrology Institute, 2024, JINST 20 P02012. DOI: https://doi.org/10.1088/1748-0221/20/02/P02012.

[2] J. Šolc, S. Pojtinger, J. Šmoldasová, V. Sochor, J. Rusňák. The spectrometric practical voltage: determination of X-ray tube voltage up to 300 kV by in-beam X-ray spectrometry with a cadmium telluride detector, 2024, JINST 20 P02013. DOI: https://doi.org/10.1088/1748-0221/20/02/P02013.

[3] J. Plagnard, Comparison of measured and calculated spectra emitted by the X-ray tube used at the Gustave Roussy radiobiological service, X-Ray Spectrometry, Vol. 43, Issue 5, pp 298-304, 2014. DOI: https://doi.org/10.1002/xrs.2554.

[4] J. Šolc, P. Dryák, J. Rusňák, V. Sochor, Z. Vykydal. Practical X-ray beam spectrometry with cadmium telluride detector in 10–300 kVp range at Czech Metrology Institute. Part II. Unfolding, 2022 JINST 17 P10003. DOI: https://doi.org/10.1088/1748-0221/17/10/P10003.

[5] J. Šolc, P. Dryák, J. Rusňák, V. Sochor, Z. Vykydal. Practical X-ray beam spectrometry with cadmium telluride detector in 10–300 kVp range at Czech Metrology Institute. Part I. Instrumentation, 2022 JINST 17 P10002. DOI: https://doi.org/10.1088/1748-0221/17/10/P10002.

[6] A. Savitzky and M. J. E. Golay, Smoothing and Differentiation of Data by Simplified Least-Squares Procedures, Analytical Chemistry, 36, 1627-1639, 1964, DOI: https://doi.org/10.1021/ac60214a047.

[7] T.J. Kennet, W.V. Prestwich, A. Robertson. Bayesian deconvolution I: convergent properties, NIM 151, 285 – 292, 1978. DOI: https://doi.org/10.1016/0029-554X(78)90502-5.

[8] G. D'Agostini. A multidimensional unfolding method based on Bayes' theorem, NIM A 362, 487 – 498, 1995. DOI: https://doi.org/10.1016/0168-9002(95)00274-X.

[9] N. Cornejo Díaz. Maximum likelihood estimation using expectation maximization applied to ambient dose equivalent measurements, Radiation Protection Dosimetry, Volume 182, Issue 2, December 2018, Pages 285–293. DOI: https://doi.org/10.1093/rpd/ncy064.

[10] M. Reginatto. The "multi-channel" unfolding programs in the UMG package: MXD_MC33, GRV_MC33 and IQU_MC33 (UMG package), version 3.3, Physikalisch-Technische Bundesanstalt, 2004.

8. Appendix

8.1 Uncertainty budget for the spectrometry method with typical values for their relative uncertainty contributions

a) Characterisation of the detector

Comparison of simulated and measured peak efficiency

Description input quantity	Relative uncertainty contribution in %	Coverage factor, k	Variable	Unit	Probability distribution	Type of uncertainty	Comments
Uncertainty on the activity of radionuclide sources used for calibration	0.7 % - 1.1 %	1	A	Bq	Normal	B	
Uncertainty of the source-to-sensor distance d_{sd} during the measurement	±2 mm/d_{sd}	1	d_{sd}	mm	Normal	B	
Uncertainty of photon yield	0.3 % - 1.2 %	1	Y			B	varies; gamma lines <0.3%, characteristic lines <1.2%
Uncertainty of photon yield	0.5 % - 1.4 %	1	Y			B	Varies depending on radionuclide. Displayed u's in photon yield are for Am-241 and Co-57 (Ref. Nucleide LNHB)
Statistical uncertainty of the net number of measured counts in full-energy peak	0.2 %	1	N		Poisson	A	
Statistical uncertainty of the net number of measured counts in full-energy peak	0.1 %	1	N		Poisson	A	Estimation using a Co-57 source
Statistical uncertainty of Monte Carlo method	0.2 %	1	N_{MC}		Normal	A	

Description input quantity	Relative uncertainty contribution in %	Coverage factor, k	Variable	Unit	Probability distribution	Type of uncertainty	Comments
Uncertainty of cross section tables used for Monte Carlo simulations	1 % - 5 %	1	s/r	cm^2/g	Normal	B	5 %, 2 %, and (1-2) % for photons with an energy of (1-5) keV, (5-100) keV, and (0.1-10) MeV respectively, for EPDL97 data used, for example, by MCNP code [Ref: D.E. Cullen et al. EPDL97: the Evaluated Photon Data Library, '97 Version," Lawrence Livermore National Laboratory, UCRL--50400, Vol. 6, Rev. 5, September 1997];

Energy calibration curve

Description input quantity	Relative uncertainty contribution in %	Coverage factor, k	Variable	Unit	Probability distribution	Type of uncertainty	Comments
Energy calibration curve	0.04 keV/E – 0.06 keV/E	1	*E*	keV		B	See for example (https://doi.org/10.1088/1748-0221/20/02/P02013, Table 2); the difference between fit and data points. The relative uncertainty is highest at low energies

Charge carrier transport

Description input quantity	Relative uncertainty contribution in %	Coverage factor, k	Variable	Unit	Probability distribution	Type of uncertainty	Comments
Charge carrier transport (CCT) in CdTe sensors	1 % - 10 %	1				B	• Charge carrier transport (CCT) in CdTe sensors influences the shape of the detector spectrum (see https://doi.org/10.1088/1748-0221/20/02/P02013 for details). Correction of Monte Carlo simulated detector response to the CCT should be included in the response matrix. • Sections 3.1.6 and Tables 6-10 in https://doi.org/10.1088/1748-0221/20/02/P02013 ("RM2", 3rd column) evaluate the uncertainty of mean energy, HVLs, and selected conversion coefficients of N-series, RQR-series, and TW-series radiation qualities, raised by neglecting the CCT transport. • The systematic uncertainty is a few % (but can be > 10% for some qualities), largest for lowest kV and low-filtered qualities.
CIEMAT - Charge carrier transport (CCT) in HP Ge spectrometers	assumed negligible					B	

Detector energy resolution

Description input quantity	Relative uncertainty contribution in %	Coverage factor, k	Variable	Unit	Probability distribution	Type of uncertainty	Comments
Detector energy resolution of a CdTe spectrometer	0.1 % - 3 % (may be higher for low-filtered, <40 kV beams)	1				B	Sections 3.1.6 and Tables 6-10 in https://doi.org/10.1088/1748-0221/20/02/P02013 ("RM3", 4th column) evaluate the uncertainty of mean energy, HVLs, and selected conversion coefficients of N-series, RQR-series, and TW-series radiation qualities, raised by neglecting the CCT transport and the detector energy resolution. The effect is smaller compared to neglecting the CCT. The systematic uncertainty is a few %, largest for low-filtered qualities.
Detector energy resolution of a HP Ge spectrometer	<0.1 %					B	

b) Energy calibration

Description input quantity	Relative uncertainty contribution in %	Coverage factor, k	Variable	Unit	Probability distribution	Type of uncertainty	Comments
CdTe detectors: visualization vs. unfolding	0.7 % (may be higher for very low kV beams)	1				B	• CCT effect in CdTe sensors causes non-symmetric full-energy peaks. Therefore, the peak maximum does not actually correspond to the energy of primary photons; it is shifted slightly to the lower energy. This should be reflected in the response matrix. • Sections 3.1.5, 3.1.6 and Tables 6-10 in https://doi.org/10.1088/1748-0221/20/02/P02013 ("RM1b", 5th column) evaluate the uncertainty of mean energy, HVLs, and selected conversion coefficients of N-series, RQR-series, and TW-series radiation qualities, raised by neglecting the energy calibration influenced by CCT transport.
Hp Ge detectors: visualization vs. unfolding	non applicable						

Description input quantity	Relative uncertainty contribution in %	Coverage factor, k	Variable	Unit	Probability distribution	Type of uncertainty	Comments
Count rate for a CdTe detector	0.1 keV/E	1				B	• Count rate in the CdTe detector influences the energy calibration. • Sections 2.9.2, 3.1.1 and Tables 6-10 in https://doi.org/10.1088/1748-0221/20/02/P02013 ("RM1c", 6th column) evaluate the uncertainty of mean energy, HVLs, and selected conversion coefficients of N-series, RQR-series, and TW-series radiation qualities, raised by the influence of count rate on energy calibration. • Suggestion: perform energy calibration at the same count rate as expected/reached during X-ray spectra measurement; perform X-ray spectra measurements at fixed count rate, for which the energy calibration is available.
Count rate for a HP Ge detector	assumed negligible						The count rate should, if possible, be kept low enough not to cause disturbances in the spectra. With Ge detectors, no shift in energy calibration as a function of the count rate has been observed, and the only source of additional uncertainty due to count rate is pile-up.
Short term stability over time of CdTe detector	0.05 keV/E	1			Uniform	B	Short term uncertainty (e.g. a few weeks). Ref. https://doi.org/10.1088/1748-0221/20/02/P02013, Table 2
Long term stability over time of CdTe detector	0.15 keV/E	1			Uniform	B	Long term uncertainty (e.g. a few months). Suggestion: perform energy calibration periodically at least once a year, preferably once per 6 months; if the energy has to be determined very precisely, perform energy calibration shortly before or after the given measurement.
Short term stability over time of HP Ge detector	0.04 keV/E	1			Uniform	B	Use of sources of Co-57 and Am-241 (follow up of FWHM with GENIE for 3 weeks)
Long term stability over time of HP Ge detector	0.19 keV/E	1			Uniform	B	Use of sources of Co-57 and Am-241 (follow up of FWHM with GENIE for 2 months)

c) Response matrix calculation

Description input quantity	Relative uncertainty contribution in %	Coverage factor, k	Variable	Unit	Probability distribution	Type of uncertainty	Comments
Statistical uncertainty of the simulations (see 8.1 a))	0.2%	1	N_{MC}		Normal	A	typical target statistical uncertainty of full-energy peaks
Uncertainty of cross section tables used for Monte Carlo simulations (see 8.1 a))	1-5%	1	s/r	cm^2/g	Normal	B	5 %, 2 %, and (1-2) % for photons with an energy of (1-5) keV, (5-100) keV, and (0.1-10) MeV respectively, for EPDL97 data used, for example, by MCNP code [Ref: D.E. Cullen et al. EPDL97: the Evaluated Photon Data Library, '97 Version," Lawrence Livermore National Laboratory, UCRL--50400, Vol. 6, Rev. 5, September 1997];

d) Unfolding/deconvolution procedure

Description input quantity	Relative uncertainty contribution in %	Coverage factor, k	Variable	Unit	Probability distribution	Type of uncertainty	Comments
Influence of the deconvolution procedure	<0.15% iterative unfolding method	1	-		-	B	From unfolding comparison performed within this activity. Peeling method could not be used in the comparison because the energy resolution of the detector was taken into account in the response matrix.

e) Measurement set-up

Description input quantity	Relative uncertainty contribution in %	Coverage factor, k	Variable	Unit	Probability distribution	Type of uncertainty	Comments
Collimator alignment to the focus point (axis of the collimator crosses the focus point on the anode) for a CdTe detector	0.2°/ref	1				B	• Sections 2.6.1 and 3.1.1 in https://doi.org/10.1088/1748-0221/20/02/P02012 • Depends on the radius of collimator aperture; smaller radius has larger influence • Estimated uncertainty of the collimator alignment is 0.2° with the setup from the paper mentioned above • Influence on the measured spectra has not been evaluated yet; • Suggestion: use >= 200 um aperture hole diameters (valid for 1 mm thick collimator), if possible. Use an alignment tool based on an X-ray projection, rather than a laser pointer (visible beam)
Tilt of collimator aperture (axis of the aperture is not parallel with the axis of the collimator) for a CdTe detector						B	• Sections 2.8 and 3.1.2 in https://doi.org/10.1088/1748-0221/20/02/P02012 • Depends on the radius of collimator aperture and the collimator thickness; relevant for diameters up to about 100 um (1 mm thick); relevant for spectra generated with > 35 kV. • For 100 um diameter aperture, HVL reproducibility is +- 0.6% for RQR10 (150 kV) with the setup from the paper mentioned above; • Suggestion: whenever possible, use >= 200 um aperture hole diameters (valid for 1 mm thick collimator).

Description input quantity	Relative uncertainty contribution in %	Coverage factor, k	Variable	Unit	Probability distribution	Type of uncertainty	Comments
Detection of scattered photons						B	• Photons scattered on the collimator body, detector construction, or on nearby objects AND not considered by response matrix • Such contribution, if not considered by response matrix, remains in the unfolded fluence spectrum and influences any quantity further calculated • Contribution strongly depends on kV, beam filtration, beam radius at the detector, collimation system, detector shielding, or mass and position of nearby objects; cannot be quantified generally. • For detectors using standard stainless steel collimator by Amptek, this effect starts to be significant for about > 70 kV radiation qualities; for > 70 kV, additional shielding is needed (unless the scatter is removed by another way e.g., response matrix) • Suggestion: avoid this uncertainty component completely by using sufficient shielding.

Limited field of view (spectrometer may not see part of photons present in the beam at the measurement position)						B	• Scattered photons: photons scattered on objects in the irradiation hall, which may be detectable by other instruments like ionization chambers, personal dosimeters, etc. This may be an advantage or disadvantage depending on the aim of the measurement.
							• Characteristic photons: characteristic photons from material present in the beam path. If the beam cross section is smaller then the field of view of the detector, then lower number of characteristic photons will be detected and the characteristic peaks will be lower.
							  ○ This has not been studied yet.
							  ○ Suggestion: use collimator with larger aperture diameter

Description input quantity	Relative uncertainty contribution in %	Coverage factor, k	Variable	Unit	Probability distribution	Type of uncertainty	• Comments
Temperature of the sensor						B	• The sensor of the CdTe detector (by Amptek) is electrically cooled down to about 220 K. The temperature may be changing during the measurement, namely at high count rates or when heat dissipation from the detector cover is insufficient. • The temperature should be kept constant (within +-1 K) and the at the same value as used during detector energy calibration. • Uncertainty was not evaluated, but the energy calibration shift was observed. • Suggestion: keep the sensor temperature constant during the measurement (use a fan cooler if necessary); keep the same temperature as during the detector calibration.

f) Other contributions - HVL determination

Description input quantity	Relative uncertainty contribution in %	Coverage factor, k	Variable	Unit	Probability distribution	Type of uncertainty	Comments
Cross sections for HVL derived from spectra	1.1 %					B	• Cross section data used for calculation of HVL • The difference between HVLs obtained using XCOM unrenormalized and PENELOPE renormalized cross sections (mu/rho for Al or Cu and mu_en/rho for air) can reach up to about 1%, namely for low energy (about <= 60 kV) wide spectra; • Suggestion: 1) state cross sections used when reporting HVLs, 2) make generally-accepted selection of one specific cross section tables to be used for HVL calculations from fluence spectra.
Method of interpolation of tabulated data						B	• Interpolation of mu/rho and mu_en/rho when calculating HVL: • Suggestion: test various interpolation methods and suggest the most suitable one (currently most promising method – cubic B-spline, done separately in every interval of smooth data between K,L,M-edges). • Interpolation of monoenergetic conversion coefficients: A lower influence on the output quantities is expected with the new monoenergetic conversion coefficients (https://doi.org/10.1088/1361-6498/adda56) published in the framework of this 22NRM07 GRP project.